

Seasonal Mean and Extreme rainfall events over India during Indian Summer Monsoon in an Indian Regional Reanalysis Framework

Deepanshu Aggarwal

MS16116

*A dissertation submitted for the partial fulfillment of
BS-MS dual degree in Science*



Indian Institute of Science Education and Research Mohali

April 2021

Certificate of Examination

This is to certify that the dissertation titled “Seasonal Mean and Extreme rainfall events over India during Indian Summer Monsoon in an Indian Regional Reanalysis Framework” submitted by Deepanshu Aggarwal (MS16116) for the partial fulfilment of BS-MS dual degree programme of the Institute, has been examined by the thesis committee duly appointed by the Institute. The committee finds the work done by the candidate satisfactory and recommends that the report be accepted.



Dr. Anoop Ambili



Dr. Baerbel Sinha



Dr. Raju Attada

(Supervisor)

Dated: April 9, 2021

Declaration

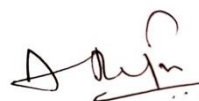
The work presented in this dissertation has been carried out by me under the guidance of Dr. Raju Attada at the Indian Institute of Science Education and Research Mohali. This work has not been submitted in part or in full for a degree, a diploma, or a fellowship to any other university or institute. Whenever contributions of others are involved, every effort is made to indicate this clearly, with due acknowledgement of collaborative research and discussions. This thesis is a bonafide record of original work done by me and all sources listed within have been detailed in the bibliography.



Deepanshu Aggarwal
(Candidate)

Dated: April 9, 2021

In my capacity as the supervisor of the candidate's project work, I certify that the above statements by the candidate are true to the best of my knowledge.



Dr. Raju Attada
(Supervisor)

Acknowledgements

First and foremost, praise and thanks to God for his showers of blessings throughout my thesis work to complete the thesis successfully.

I would like to express my deep and sincere gratitude to my thesis supervisor, Dr. Raju Attada for giving me the opportunity to work under his guidance and providing invaluable guidance and support throughout this thesis. His dynamism, sincerity, kindness and motivation have deeply inspired me. It was a great privilege and honour to work and study under his guidance.

I also thank the members of my dissertation committee, Dr. Baerbel Sinha and Dr. Anoop Ambili for their constant support, encouragement, constructive criticism and direction during the course of this dissertation.

My sincere thanks to Dr. Krishna Kumar Shukla for his help and guidance with the thesis work. I also thank him for his warm hospitality. I express my thanks to all my lab mates of the Weather and Climate Modeling Group, especially Nischal, Rohtash and Abhishek for their unconditional support and constructive discussions.

I would like to extend my thanks to my university, especially the dept. of EES , Computer Centre and the Library for providing valuable resources to complete my thesis.

I am extremely grateful to my parents for their love, prayers, caring and sacrifices for educating and preparing me for my future. I am very much thankful to my brother for his constant support.

List of Figures

Figure 1: Spatial distribution of monthly (June, July, August & September) and seasonal (JJAS) precipitation characteristics (mm/day) from CPC (a-e), IMD (f-j), IMDAA (k-o) and TRMM (p-t) with time period being 1979-2018 for IMD, CPC and IMDAA and 1998-2018 for TRMM	11
Figure 2: Daily climatology of rainfall over MCR (a) and Northwest India (b) as captured by CPC, IMD, IMDAA and TRMM. Correlations between the daily climatology by IMDAA and other datasets i.e., IMD, CPC, TRMM over MCR (c-e) and Northwest India (f-h).....	12
Figure 3: Peak times (0: midnight to 23: 11 pm) of total, convective and stratiform precipitation during ISM from IMDAA (a, b and c) and ERA5 (e, f and g). Ratio of convective precipitation to total precipitation on an average day during ISM as captured by IMDAA (d) and ERA5 (h). Precipitation includes both rainfall and snowfall.....	14
Figure 4: Seasonal (JJAS) precipitation trends (mm/day/year) as produced by IMD (a), CPC (b), IMDAA (c) and TRMM (d). Dots represent trends with 95% significance level. Data period for TRMM is 1998-2018 (21 years), while for others it is, 1979-2018 (40 years).....	17

Figure 5: Trends in area-averaged seasonal mean precipitation over MCR (a) and Northwest India (b) as produced by IMDAA, IMD, CPC and TRMM. Data period for TRMM is 1998-2018 (21 years) while for others it is, 1979-2018 (40 years)..... 18

Figure 6: Monthly (June, July, August and September) mean precipitation trends (mm/day/year) as produced by IMD (a-d), IMDAA (e-h), CPC (i-l) and TRMM (m-p). Cross markers (x) indicate trends with 95% significance level. Data period for TRMM is 1998-2018 (21 years) while for others it is, 1979-2018 (40 years)..... 19

Figure 7: Spatial distribution of mean winds at 200 hPa (m/s), 850 hPa (m/s) and mean sea level pressure (MSLP; hPa) from IMDAA (a, b and c) and ERA5 (d, e and f) for the period 1979-2018. The difference between the two datasets is plotted (g, h and i)..... 20

Figure 8: Mean ISM vorticity at 850 hPa (s^{-1}) and vertically integrated (between 1000 and 200 hPa) moisture transport ($kg\ m^{-1}\ s^{-1}$) as captured by IMDAA (a and b), ERA5 (c and d) and the difference between two datasets (e and f)..... 21

Figure 9: Mean ISM tropospheric temperature (between 700 and 200 hPa) as captured by IMDAA (a), ERA5 (b) and the difference between the two (c)..... 22

Figure 10: Mean meridional distribution of easterly wind shear (a), tropospheric temperature (b) and vertically integrated specific humidity (c) averaged between 60°E and 100°E during ISM as captured by IMDAA (solid blue) and ERA5 (solid red). (d) Vertical profile of diabatic heating over MCR (solid black) and Northwest India(dashed black) during ISM as captured by ERA5..... 23

Figure 11: Linear trends in frequency of EREs (more than 150 mm/day) and widespread events over MCR as produced by IMD (a and b) and IMDAA (c and d). The box in a and c represent the MCR region taken to calculate the widespread events in b and d. Trend values are in $\text{mm day}^{-1} 40 \text{ year}^{-1}$ 25

Figure 12: Winds at 850 hPa (m/s) and 200 hPa (m/s) during widespread events over MCR from IMDAA (a and b) and IMD (c and d). The difference between the two is also plotted (e and f).....26

Figure 13: Vorticity at 850 hPa (s^{-1}) and VIMT for 1000 to 200 hPa ($\text{kg m}^{-1} \text{s}^{-1}$) during widespread events over MCR from IMDAA (a and b) and IMD (c and d). The difference between the two is also plotted (e and f). 27

Figure 14: Linear trends in frequency of EREs (more than 109 mm/day) and widespread events over Northeast India from IMD (a and b) and IMDAA (c and d). The box in a and c represent the Northwest India region taken to calculate the widespread events in b and d. Trend values are in $\text{mm day}^{-1} 40 \text{ year}^{-1}$ 28

Figure 15: Winds at 850 hPa (m/s) and 200 hPa (m/s) during widespread events over Northwest India from IMDAA (a and b) and IMD (c and d). The difference between the two is also plotted (e and f)..... 29

Figure 16: Vorticity at 850 hPa (s^{-1}) and VIMT for 1000 to 200 hPa ($\text{kg m}^{-1} \text{s}^{-1}$) during widespread events over Northwest India from IMDAA (a and b) and IMD (c and d). The difference between the two is also plotted (e and f). 30

List of Tables

Table 1: Datasets used in this study.....	5
Table 2: A contingency table.....	7
Table 3: Statistics for examination of IMDAA's ability to detect low, moderate and heavy rainfall events against that of IMD and CPC over MCR.....	15
Table 4: Statistics for examination of IMDAA's ability to detect low, moderate and heavy rainfall events against that of IMD and CPC over Northwest India.....	15
Table 5: Performance measures of IMDAA against IMD and CPC for ISM during 1979-2018.....	16

Notation (Abbreviations)

CPC	Climate Prediction Centre
ECMWF	European Centre for Medium-Range Weather Forecasts
EREs	Extreme Rainfall Events
GCM	Global Climate Model
GDP	Gross Domestic Product
IMD	India Meteorological Department
IMDAA	Indian Monsoon Data Assimilation and Analysis
ISM	Indian Summer Monsoon
MCR	Monsoon Core Zone
MCS	Monsoon Convective System
MSLP	Mean Sea Level Pressure
NOAA	National Oceanic and Atmospheric Administration
SST	Sea Surface Temperature
TRMM	Tropical Rainfall Measuring Mission
VIMT	Vertically Integrated Moisture Transport
WMO	World Meteorological Organization

Contents

List of Figures.....	i
List of Tables.....	v
Abstract.....	xi
1. Introduction.....	1
2. Materials and Methods.....	4
2.1. Data.....	4
2.2. Calculation of unavailable variables from available ones.....	5
2.3. Identification of EREs.....	6
2.4. Performance Statistics.....	7
3. Results.....	10
3.1. Indian Summer Monsoon (ISM) mean precipitation characteristics.....	10
3.2. Large scale Circulation characteristics of ISM.....	19
3.3. Extreme rainfall events (EREs) during ISM.....	23
4. Conclusions.....	31
Bibliography.....	33

Abstract

Indian Summer Monsoon (June-September) Rainfall (ISMR) over the Indian subcontinent accounts for more than 70% of annual rainfall, which is crucial for socioeconomic development and well-being of this densely populated region of the world. Understanding the finer details of rainfall distribution is also important for many sectors such as agriculture and water resource management. Further, the spatio-temporal variability of monsoon rainfall processes, especially the extreme rainfall events (EREs) over India is quite complex due to its variable topography, availability of moisture sources and circulation patterns. Northwest India, the ‘breadbasket’ of the country along with Central India are home to a significant fraction of Indian population and intensive urbanization which makes them extremely vulnerable to ramifications of EREs such as flash floods, landslides, agricultural and infrastructural damages, including significant loss of human and animal lives. Such events and the associated variability are in general expected to increase owing to climate change.

There are limited reports on the characteristics of EREs over Northwest Indian region. Central India (Monsoon Core Region-MCR), on the other hand has got significant scientific attention but it is yet to be viewed from the eyes of the highest resolution first ever regional atmospheric reanalysis over India, Indian Monsoon Data Assimilation and Analysis reanalysis (IMDAA). Therefore, this forms the main motivation to examine the EREs over Northwest and MCR during Indian Summer Monsoon for the period 1979 to 2018 using precipitation data from India Meteorological Department (IMD) and IMDAA reanalysis available at spatial grid of $0.25^\circ \times 0.25^\circ$ and 12 km, respectively.

Further, the state-of-the-art IMDAA reanalysis precipitation data has been compared with data from IMD, CPC and TRMM using standard statistical skill scores. Our results reveal that IMDAA produces better spatial rainfall distribution compared to IMD data at monthly

and seasonal time scales but rainfall patterns indicate varying degrees of overestimation all over the country. IMDAA realistically represent the ISM salient features such as cross-equatorial flow, low-level jet, monsoon trough, tropical easterly jet, and finer rainfall distribution details. Furthermore, EREs and widespread events from IMD and IMDAA exhibit significant quantitative differences in terms of spatio-temporal trends. IMDAA well captures the regional trends in widespread EREs. Our study critically evaluates the proficiency of newly released high resolution IMDAA reanalysis over Indian subcontinent and its competency in terms of representation of monsoonal features with a global reanalysis, ERA5. With trend analysis of EREs and widespread events, our study will further provide inputs in terms of expected future evolution of monsoon precipitation and extreme rainfall events which could help in mitigation policy framework and infrastructure designing.

Chapter 1

Introduction

Monsoon onset occurs over the southwestern tip of Indian peninsula around the beginning of June and the entire country comes under the euphoria of monsoon by mid-July. It retreats from most of the country by the month of October, however, it leaves the southwestern tip of India only by December. This period is divided into two seasons: the southwest monsoon (surface winds are from southwest) from June to September and; the northeast monsoon (surface winds are from northeast) from October to December (e.g. Gadgil, 2018). Southwest monsoon aka Indian Summer Monsoon (ISM) lasts for about 4 months (June to September) and makes for 60-90% of annual rainfall over India (e.g. Shukla & Huang, 2016). Monsoon brings much awaited relief from extreme pre-monsoon temperatures, waters the crops, revives rivers and aquifers. It is what sustains the Indian agriculture that accounts for about 18% of GDP and employs 52% of the population (e.g. Arjun, 2013).

On the other hand, the Extreme Rainfall Events (EREs) associated with ISM are a cause of concern since they can be a cause of flash floods, landslides, crop and infrastructural damage, loss of human & animal lives and their displacement (Goswami et al., 2006; Roxy et al., 2017). EREs in general have high spatio-temporal variability and this can be further enhanced if these events are associated with the ISM, which is highly chaotic in nature. The threat of climate change and rising tropical sea surface temperatures (SSTs) poses a new dimension of uncertainty in prediction of ISM rainfall (Kulkarni et al., 2020; Roxy et al., 2017). This calls for more concentrated research on ISM given its immense importance both for Indian climate and the global atmospheric general circulation system. Numerous

studies have pointed towards the increasing trends of frequency and magnitude of EREs during ISM and attributed it to climate change (Goswami et al., 2006; Kulkarni et al., 2020; Roxy et al., 2017; Roy & Balling, 2004). Many simulations have shown similar results however with an increasing trend in monsoon low pressure areas (LPAs) in contrast to observations showing decrease in such LPAs (Roxy et al., 2017). Therefore, a proper assessment of likely future trends is vital in order to set up infrastructure for disaster preparedness (Goswami et al., 2006).

Northwest India, known as the ‘breadbasket’ of our country, receives 50%-75% of their total annual rainfall during ISM (Halpert & Bell, 1997), however, isolated EREs are more pronounced. The region has limited studies and that too showing contrasting results in trends of EREs over this region (Malik et al., 2016; Roy & Balling, 2004). This makes northwest India as our primary region of interest. Monsoon core region (MCR) has also been analysed since it receives more than 90% of its total annual precipitation (Halpert & Bell, 1997). Though, MCR has got abundant scientific attention and has been investigated by numerous studies, we here use the highest resolution first ever regional atmospheric reanalysis over India, Indian Monsoon Data Assimilation and Analysis reanalysis (IMDAA) to confirm the signatures of EREs.

Gridded precipitation datasets are widely used in climate research and analysis of spatio-temporal variations. Quality of datasets exclusively based on surface gauge network depends on “gauge density and distribution, the procedure to quality control the raw data, and the analysis scheme to get data at grid points from irregularly distributed gauges” and therefore, such datasets are “generally biased towards populated areas and against regions of high elevation, complex terrain, and arid climate that are sparsely populated” (Kim et al., 2015, Introduction section). Then there are datasets based on satellite precipitation retrievals that have advantages in terms of both useful resolutions and extensive coverage, but since these are indirect measurements, errors mainly arise from retrieval algorithms used to relate the radiometric measurements with actual precipitation values (Kim et al., 2015). It has been reported that a long term, high-quality, physically consistent multivariate data is essential to better understand rainfall distribution and climate variability (Zhang et al., 2017). These qualifications are fulfilled by reanalysis datasets that merge observations

from sparse locations into a modeling framework and create a consistent, coherent, comprehensive and uniformly gridded meteorological data set (Ashrit et al., 2020; Zhang et al., 2017). However, since global reanalysis needs enormous human effort, computing power and storage capacity, they are generated at moderate grid resolutions which in turn impedes their applications in weather and climate studies at the local and regional scales since they provide inadequate descriptions of regional synoptic & mesoscale processes while climatic extreme incidents such as mesoscale convective systems, tropical cyclones, regional droughts and heat waves need high spatial and temporal resolutions (Ashrit et al., 2020; Raju et al., 2015; Zhang et al., 2017). With reference to monsoon, a study using a variable resolution global general circulation model (GCM), with telescopic zooming and enhanced resolution (*35 km) over South Asia demonstrated that the high resolution greatly improves the simulation of ISM precipitation and circulation characteristics over the Indian region (P Sabin et al., 2013). Thus, for a more detailed analysis of weather parameters, we make use of regional reanalysis. Regional reanalysis utilizes the high-resolution models with limited spatial coverage that derive initial and boundary conditions from a global reanalysis. The regional reanalysis provides more information for accurate analysis by including additional physical parameterizations and local details (Attada et al., 2018; Zhang et al., 2017).

Here, we have used recently released highest resolution (12 km) regional atmospheric reanalysis, IMDAA reanalysis over Indian subcontinent to investigate mean and extreme precipitation trends and explore associated atmospheric circulation patterns over India, specifically focusing over Northwest India and MCR. The IMDAA reanalysis is generated in collaboration by Met Office of UK, National Centre for Medium Range Weather Forecasting (NCMRWF) of India and the India Meteorological Department (IMD) of India with funding from the National Monsoon Mission project of the Ministry of Earth Sciences, Government of India (Ashrit et al., 2020; Rani et al., 2021). IMDAA derives its lateral boundary conditions from the global reanalysis ERA-Interim and includes a wide range of observations from land, sea, radiosondes, pilot balloons, aircrafts and various satellite instruments (Ashrit et al., 2020). Our main aim of this work is to explore the regional-to-local distribution of ISMR and their spatio-temporal trends over the MCR and Northwest Indian regions after extensive validation of IMDAA reanalysis using different gridded (e.g., IMD) and global reanalysis (e.g., ERA5) products.

Chapter 2

Materials and Methods

2.1. Data

We have used multiple gridded, global and regional reanalysis datasets. IMD's high resolution ($0.25^\circ \times 0.25^\circ$) daily gridded rainfall data set over India is used as a representation of 'ground truth'. This is plausible because of two reasons. First, though, uncertainties in rainfall estimates are of major importance for hydrologists since they directly affect calculations of stream flows and calibration of hydrology models, these uncertainties are of least concern while producing rainfall trends and patterns (Kim et al., 2015). Secondly, IMD gridded precipitation analysis data is based on conditional sampling from quite uniform station network in India as compared to gridded data products from other agencies (Kim et al., 2015). Hence, this is used for validation of newly released high-resolution (12 km) IMDAA reanalysis precipitation data. Additionally, NOAA Climate Prediction Centre (CPC) Global Daily Unified Gauge-based Precipitation data product and Tropical Rainfall Measuring Mission (TRMM) 3B42 daily precipitation estimates have also been used for inter-comparison (Table 1). All the datasets have been used for the period 1979-2018 except for TRMM, which is for the period 1998-2018. Recently released fifth generation ECMWF reanalysis, ERA5 (Hersbach et al., 2020) global reanalysis data has been used for comparison of IMDAA's ability to capture atmospheric circulation characteristics during ISM. Specific humidity is not provided by IMDAA and has been calculated from its relative humidity (RH) and temperature (T) using the procedure described in section

2.2.1. Our main study regions are MCR (19° -26° N; 75° -85° E) and Northwest India (28° -33° N; 74° -78° E).

Table 1: Datasets used in this study.

Dataset	Spatial coverage	Temporal coverage	Resolution	
			Spatial	Temporal
IMD daily precipitation gridded rain gauge dataset	India	1979-2018	0.25° x 0.25°	Daily
NOAA CPC (Climate Prediction Centre) Global Daily Unified Gauge-based Precipitation data product	Land	1979-2018	0.5° x 0.5°	Daily
TRMM daily precipitation dataset	Tropics (50° N-50° S)	1998-2018	0.25° x 0.25°	Daily
IMDAA (Indian Monsoon Data Assimilation and Analysis) reanalysis	South Asia + adjoining regions	1979-2018	12 km	1 hourly
ERA5 reanalysis	Global	1979-2018	0.25° x 0.25°	1 hourly

2.2. Calculation of unavailable variables from available ones

2.2.1. Specific humidity

Specific humidity can be calculated from vapour pressure and air pressure using,

$$\text{Specific Humidity}(q) \approx \varepsilon \frac{e}{p},$$

where, $\varepsilon = 0.622$, e is the vapour pressure and p is the air pressure. To find vapour pressure, we make use of a standard procedure to calculate water vapour from

radiosonde data (Rao et al., 2009). Since, Relative humidity (RH) and temperature (T) are available, we use following relations to derive vapour pressure at each pressure level:

$$RH = \frac{e}{e_s} \times 100 ,$$

$$e_s = e_{st} 10^Z ,$$

$$Z = A \left(\frac{T_s}{T} - 1 \right) + B \times \log_{10} \left(\frac{T_s}{T} \right) - C \times \left[10^{D \left(1 - \frac{T}{T_s} \right)} - 1 \right] + F \times \left[10^{H \left(\frac{T_s}{T} - 1 \right)} - 1 \right] ,$$

where, $A = -7.90298$, $B = 5.02808$, $C = -1.3816 \times 10^{-7}$, $D = 11.344$, $F = 8.1328 \times 10^{-3}$, $H = -3.49149$ and $e_{st}(1013.246 \text{ mb})$ is saturation vapour pressure (e_s) at boiling temperature ($T_s = 373.16 \text{ K}$) at standard atmospheric pressure (1013.246 mb).

2.2.2. Diabatic heating

The diabatic heating at any position in space can be calculated by using the given formula utilizing variables such as temperature (T), horizontal velocity (V), vertical velocity (ω) and pressure (p) (e.g. Mukhopadhyay et al., 2010):

$$\text{Potential Temperature } (\theta) = T \left(\frac{p_o}{p} \right)^k ,$$

$$\text{Diabatic heating} = C_p \left(\frac{p}{p_o} \right)^k \left(\frac{\partial \theta}{\partial t} + V \cdot \nabla \theta + \omega \frac{\partial \theta}{\partial p} \right) ,$$

where, $k = R/C_p$, R is the gas constant, C_p is the specific heat at of dry air at constant pressure, $p_o = 1000 \text{ hPa}$ and ∇ is the isobaric gradient operator.

2.3. Identification of EREs

Threshold for extreme rainfall events over the study region have been identified by averaging the 99.9th percentile of each grid point as produced by IMD data. Widespread events are identified as days with EREs occurring simultaneously at 10 or more grid points inside the study region, in line with Roxy et al., (2017). To look into the significance of linear trends in mean rainfall and extreme rainfall events, linear fit regression has been used.

2.4. Performance Statistics

We have used standard statistical measures to evaluate the performance of IMDAA rainfall against its counterparts such as IMD and CPC. An event is the total precipitation in a day averaged over a particular area of interest such as Northwest (Arid climate type) and MCR (Wet climate type). It is to be noted that TRMM is not used as it is available only after 1998 while others are from 1979.

2.4.1. Treating IMDAA as a forecast and IMD & CPC as observations, we derive the categorical statistics generally used to verify dichotomous (yes/no) forecasts. We have categorized the events into low (less than 5mm/day), moderate (between 5 and 25 mm/day for MCR; between 5 and 30 mm/day for Northwest India) and heavy (more than 25 mm/day for MCR; more than 30 mm/day for Northwest India) rainfall events. For each category, a contingency table is prepared (Table 2.1) and then following statistics are derived (Mcbride & Ebert, 2000; Thornes & Stephenson, 2001; <https://www.cawcr.gov.au/projects/verification/>):

Table 2: A contingency table.

Forecast	Observation			
		Yes	No	Total
	Yes	Hits (H)	False Alarms (F)	Forecast Yes
	No	Misses (M)	Correct Negatives (CN)	Forecast No
	Total	Observed Yes	Observed No	Total (N)

- a. Probability of Detection (POD): The probability of detection (POD) is equal to the number of hits divided by the total number of event observations. It ranges from 0 to 1 with 1 being the perfect score. Thus, it gives a simple measure of the proportion of rain events successfully forecasted or in this case, captured by IMDAA.

$$POD = \frac{H}{M + H}$$

- b. False Alarm Ratio (FAR): The false alarm ratio (FAR) is equal to the number of false alarms divided by the total number of times the event forecasted. The range of this score is 0 to 1 with 0 being the perfect score. It gives a simple proportional measure of IMDAA's tendency to capture the event where none was observed.

$$FAR = \frac{F}{F + H}$$

- c. Miss Rate: Miss rate is the ratio of total misses to the total event observations. It ranges from 0 to 1 with 0 being the perfect score.

$$Miss\ rate = \frac{M}{M + H}$$

- d. Critical Success Index (CSI): The CSI, also known as threat score, is the ratio of number of hits to all events either observed or captured by IMDAA. CSI ranges from 0 to 1 with 1 being the perfect score.

$$CSI = \frac{H}{H + M + F}$$

- e. Heidke Skill Score: Heidke skill score is a measure of skill in the forecast. The range of the HSS is $-\infty$ to 1. Negative values indicate that the chance forecast is better, 0 means no skill, and a perfect forecast obtains an HSS of 1.

$$HSS = \frac{(H + CN) - (Expected\ Correct)}{N - (Expected\ Correct)}$$

where,

$$Expected\ Correct = \frac{1}{N}[(H + M)(H + F) + (CN + M)(CN + F)] .$$

2.4.2. Then we calculate the standard statistics used widely for quantitative assessment of consensus between different datasets (Perez et al., 2016; Zandler et al., 2019). Here, x_i is the area averaged precipitation in one day over the study region as captured by IMDAA, \bar{x} is the mean of all x_i with n being the total number of values. Similarly, y_i is the area averaged precipitation in one day over the study region as captured by other datasets such as IMD or CPC with \bar{y} being the mean of all y_i :

- a. Coefficient of determination (R^2): R^2 ranges from 0 to 1 and is simply calculated as the square of Pearson correlation coefficient. The application of R^2 is limited as it depends on the data distribution which makes it

sensitive to outliers. Therefore, other parameters such as RMSE, MAE etc are also considered along with it generally.

$$R^2 = \left[\frac{\sum_{i=1}^n (x_i - \bar{x})(y_i - \bar{y})}{\sqrt{\sum_{i=1}^n (x_i - \bar{x})^2 \sum_{i=1}^n (y_i - \bar{y})^2}} \right]^2$$

- b. Root mean squared error (RMSE): RMSE is a frequently used measure of the differences between values captured by two datasets.

$$RMSE = \sqrt{\frac{\sum_{i=1}^n (x_i - y_i)^2}{n}}$$

- c. RMSErel:

$$RMSE_{rel} = \frac{RMSE}{\bar{x}} \times 100$$

- d. Mean Absolute Error (MAE):

$$MAE = \frac{1}{n} \sum_{i=1}^n |x_i - y_i|$$

- e. MAErel:

$$MAE_{rel} = \frac{MAE}{\bar{x}} \times 100$$

- f. BIAS:

$$BIAS = \frac{1}{n} \sum_{i=1}^n (y_i - x_i)$$

- g. BIASrel:

$$BIAS_{rel} = \frac{BIAS}{\bar{x}} \times 100$$

- h. Index of Agreement (IOA): IOA varies between 0 and 1 with 1 being a perfect match, and 0 indicating no agreement at all.

$$IOA = 1 - \frac{\sum_{i=1}^n (x_i - y_i)^2}{\sum_{i=1}^n (|y_i - \bar{x}| + |x_i - \bar{x}|)^2}$$

Chapter 3

Results

3.1. Indian Summer Monsoon (ISM) mean precipitation characteristics

Indian summer monsoon greets Indian state of Kerala on 1 June on an average with a standard deviation of 8 days (Soman & Kumar, 1993). From earlier being simply based on rainfall, IMD's criteria for declaring monsoon onset over Kerala (MOK) now uses a comprehensive perspective involving sharp increase in rainfall over Kerala along with wind fields and Outgoing Longwave Radiation (OLR) values (India Meteorological Department; Misra et al., 2018). Monsoon progress dates for other regions are declared more subjectively by considering sharp increase in rainfall, its sustenance as well as associated changes in atmospheric circulation features (India Meteorological Department). Gradually covering the entire country over a span of next 6 weeks, the monsoon is at its peak during July and August (active phase of monsoon) with huge spatial and temporal variations. The withdrawal begins with the receding of rainfall from the northwest part of India after 1 September. The southwest monsoon starts withdrawing from the extreme Northwest portion of India by the beginning of September (Kulkarni et al., 2020). The withdrawal is rather slower than onset and by 1 October, though monsoon is gone from northern parts of the country, it completely leaves the country only around 15 October.

3.1.1. Climatology perspective

A. Spatial pattern of rainfall:

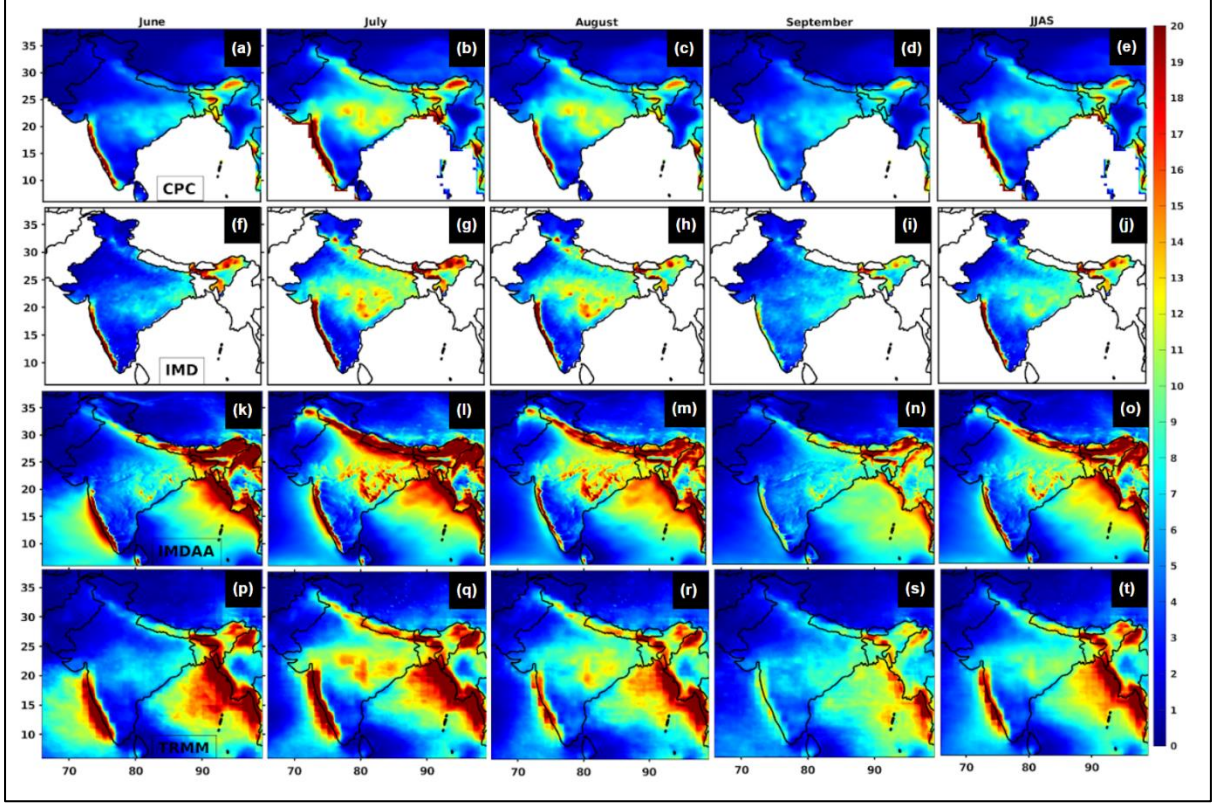


Figure 1: Spatial distribution of monthly (June, July, August & September) and seasonal (JJAS) precipitation characteristics (mm/day) from CPC (a-e), IMD (f-j), IMDAA (k-o) and TRMM (p-t) with time period being 1979-2018 for IMD, CPC and IMDAA and 1998-2018 for TRMM.

Figure 1 shows the mean spatial distribution of precipitation climatology for the period 1979-2018 (1998-2018 for TRMM) during each month and whole season of ISM across India. IMDAA successfully captures the observed major monsoon convective rainfall zones such as monsoon core region (MCR), high precipitation over western ghats, northeast regions and Himalayan foothills due to orographic and low precipitation over west & northwest regions, eastern ghats, Jammu & Kashmir and Ladakh. Rain shadow over the Southern Peninsula is well captured with finer details by IMDAA. It also successfully produces the seasonal evolution of monsoon rainfall: low rainfall in June, high rainfall during peak monsoon months (July and August) and the withdrawal phase of rainfall in September with

some significant discrepancies. This overestimation could be attributed to high spatial resolution of the IMDAA (12 Km) as it can pick up small scale vortices and associated local rainfall. Further, evaluation of rainfall over the oceans using TRMM rainfall data reveals IMDAA showing low precipitation over Bay of Bengal and Arabian Sea as compared to TRMM during ISM.

B. Seasonal Cycle of daily rainfall:

The daily climatology of ISM rainfall over Monsoon Core Region (MCR) and Northwest India is well represented by IMDAA, though clearly a lot wetter than other datasets, especially over Northwest India (Figure 2). IMDAA successfully captures the onset, peak and withdrawal phases of ISM in comparison with other datasets. The coefficient of determination for daily climatology displays high (0.96) and good (0.81) agreements between IMDAA and IMD for MCR and northwest India, respectively. CPC and TRMM show relatively low agreement with IMDAA than that between IMDAA and IMD but they still are in high range for MCR and good range for Northwest India.

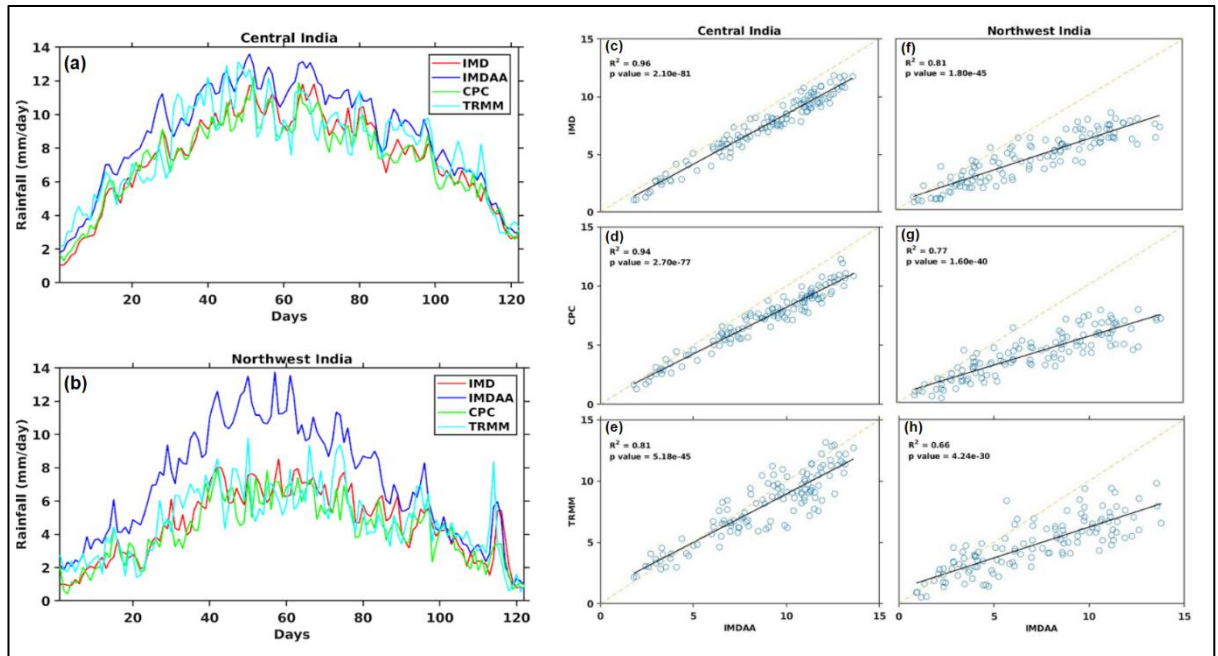


Figure 2: Daily climatology of rainfall over MCR (a) and Northwest India (b) as captured by CPC, IMD, IMDAA and TRMM. Correlations between the daily climatology by IMDAA and other datasets i.e., IMD, CPC, TRMM over MCR (c-e) and Northwest India (f-h).

C. Evaluation of convective and stratiform precipitation contribution to total monsoon rainfall:

Precipitation in tropics generally happens through mesoscale convective systems (MCSs) which can be separated into two distinct regions: convective and stratiform (Hong et al., 1999). Convective regions have strong vertical winds and higher precipitation rates while stratiform regions have weak vertical air motion and low precipitation rate barely exceeding 10 mm/hr (Hong et al., 1999; Lang et al., 2003). These regions also possess considerably different vertical profiles of latent heat release with the convective region heating the entire troposphere while the stratiform region generally cooling the lower troposphere through evaporative cooling (Hong et al., 1999; Lang et al., 2003; Schumacher & Houze, 2003). The latent heat release associated with tropical precipitation provides the major source of energy for driving global atmospheric circulation, which makes accurate estimates of tropical precipitation and latent heat release vital for improving our understanding of large-scale climate variability. Figure 3 (a to c and e to g) show the time during an average ISM day when total, convective and stratiform precipitation was at its maximum. The peak time of convective precipitation highly resembles that of the total precipitation indicating that over India, the convective component makes more of the total precipitation than stratiform precipitation type. This is confirmed by the ratio of convective to total precipitation (Figure 3 d and h). IMDAA shows that convective makes majority of total precipitation both over Northwest and MCR in contrast to ERA5 which shows that stratiform makes a significant portion of total precipitation over MCR. Moreover, there is a large difference in peak timings of IMDAA and ERA5 across India though peninsular India shows some agreement. This peak timing of diurnal scale precipitation is quite complex which further needs to be checked with available remote sensing data.

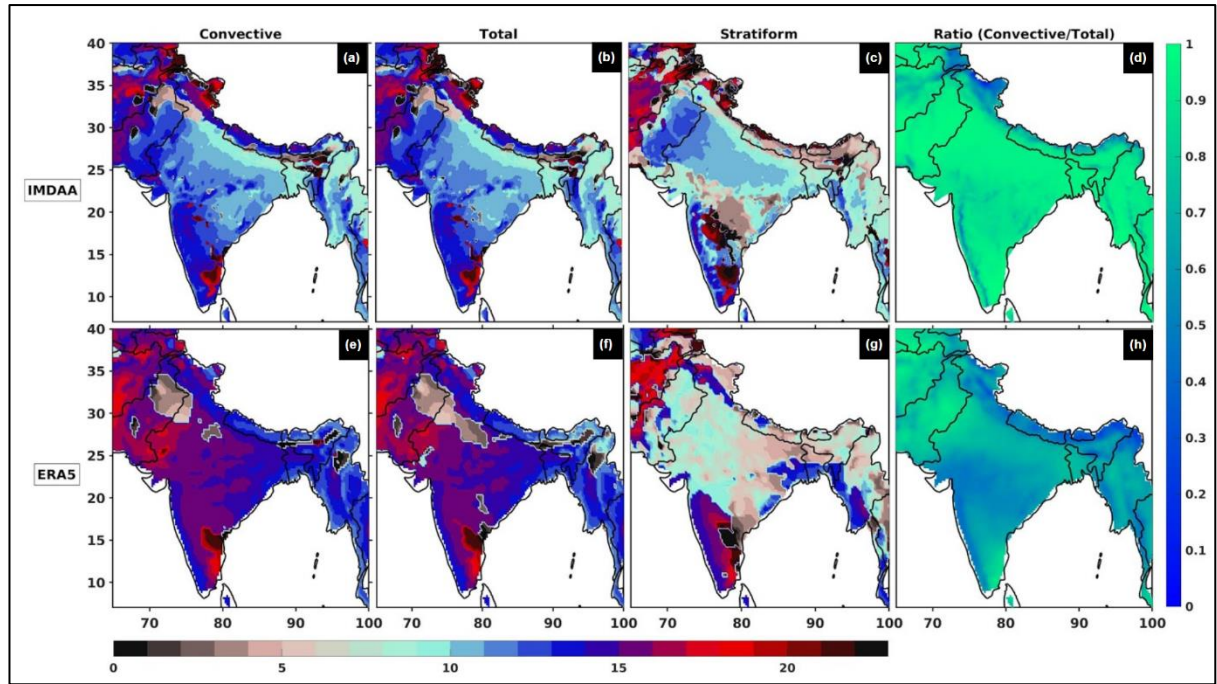


Figure 3: Peak times (0: midnight to 23: 11 pm) of total, convective and stratiform precipitation during ISM from IMDAA (a, b and c) and ERA5 (e, f and g). Ratio of convective precipitation to total precipitation on an average day during ISM as captured by IMDAA (d) and ERA5 (h). Precipitation includes both rainfall and snowfall.

3.1.2. IMDAA performance statistics

Table 3 and 4 show some categorical statistics derived by treating IMDAA as a forecast for comparison with IMD and CPC which are treated as observation datasets. For MCR (Table 3), IMDAA shows a high probability of detection of low (<5 mm/day) and moderate (between 5 and 25 mm/day) rainfall events in both IMD and CPC. Correspondingly, FAR and miss rate are low while CSI is in good range. The skill is quite opposite for heavy (>25 mm/day) rainfall events with low POD and CSI and high FAR and miss rate. Heidke skill score, a measure of IMDAA's skill to predict events observed by IMD and CPC, shows that IMDAA has good skills for capturing low and moderate rainfall events but poor for heavy rainfall events. For Northwest India (Table 4), IMDAA shows good, high and low probability of detection of low, moderate (between 5 and 30 mm/day) and heavy (>30 mm/day) events, respectively, with both IMD and CPC. False alarm ratio is low for low rainfall events but high for moderate and heavy rainfall events with both IMD and CPC. Miss rates are lowest for moderate rainfall events and highest

for heavy rainfall events. Heidke skill score lies almost halfway of no skill (0) and perfect skill (1) for low and moderate rainfall events with both IMD and CPC. For heavy rainfall events, IMDAA shows a poor skill with both IMD and CPC.

Table 3: Statistics for examination of IMDAA's ability to detect low, moderate and heavy rainfall events against that of IMD and CPC over MCR.

MCR						
		POD	FAR	Miss Rate	CSI	HSS
IMD	Low	0.74	0.14	0.26	0.66	0.7
	Moderate	0.9	0.15	0.1	0.77	0.65
	Heavy	0.4	0.84	0.6	0.13	0.22
CPC	Low	0.67	0.15	0.33	0.6	0.6
	Moderate	0.9	0.22	0.11	0.71	0.57
	Heavy	0.4	0.75	0.6	0.18	0.3

Table 4: Statistics for examination of IMDAA's ability to detect low, moderate and heavy rainfall events against that of IMD and CPC over Northwest India.

Northwest India						
		POD	FAR	Miss Rate	CSI	HSS
IMD	Low	0.67	0.07	0.33	0.63	0.48
	Moderate	0.85	0.46	0.15	0.5	0.45
	Heavy	0.27	0.86	0.72	0.1	0.17
CPC	Low	0.61	0.07	0.38	0.58	0.37
	Moderate	0.82	0.58	0.18	0.38	0.33
	Heavy	0.24	0.74	0.75	0.14	0.24

Table 5 contains performance statistics of IMDAA against IMD and CPC in terms of area averaged daily rainfall during ISM over the study regions of MCR and Northwest India. R^2 between IMDAA and others is higher over MCR as compared

to Northwest India. Correspondingly, RMSE is more over Northwest India than MCR. Mean absolute error and bias values are also higher over Northwest India as compared to MCR. Consequently, IMDAA shows a high index of agreement with IMD and CPC over MCR. IOA values are lower over Northwest India but still in a good range. Overall, the skill scores suggest that IMDAA yields significant skill, probably better, compared to other datasets which gives ample confidence to analyse the spatio-temporal trends in detailed.

Table 5: Performance measures of IMDAA against IMD and CPC for ISM during 1979-2018.

MCR									
Dataset	R^2	p	RMSE	RMSErel	MAE	MAErel	BIAS	BIASrel	IOA
IMD	0.66	0.00	3.91	0.44	2.80	0.32	-1.38	-0.16	0.88
CPC	0.57	0.00	4.49	0.51	3.26	0.37	-1.56	-0.18	0.85
Northwest India									
IMD	0.40	0.00	6.27	0.88	3.92	0.55	-2.50	-0.35	0.75
CPC	0.34	0.00	7.11	1.00	4.63	0.65	-2.88	-0.41	0.73

3.1.3. Trends in mean monsoon precipitation

Figure 4 shows the linear trends in mean ISM precipitation (mm/day) across India by different datasets. IMDAA, CPC and TRMM show homogenous increasing trend over Northwest India while IMD shows mixed trends during ISM. For MCR, IMD, CPC and TRMM show almost similar picture of mixed trends over entire region except increasing trends over coastal areas of Orissa and Andhra Pradesh while IMDAA shows significant increasing trends over most of the MCR. IMD, IMDAA and TRMM show decreasing trend in mean ISM precipitation over Himalayan foothills and regions of Northeast India. All the datasets show an increasing trend for the states of Rajasthan & Gujarat and upper Western Ghats.

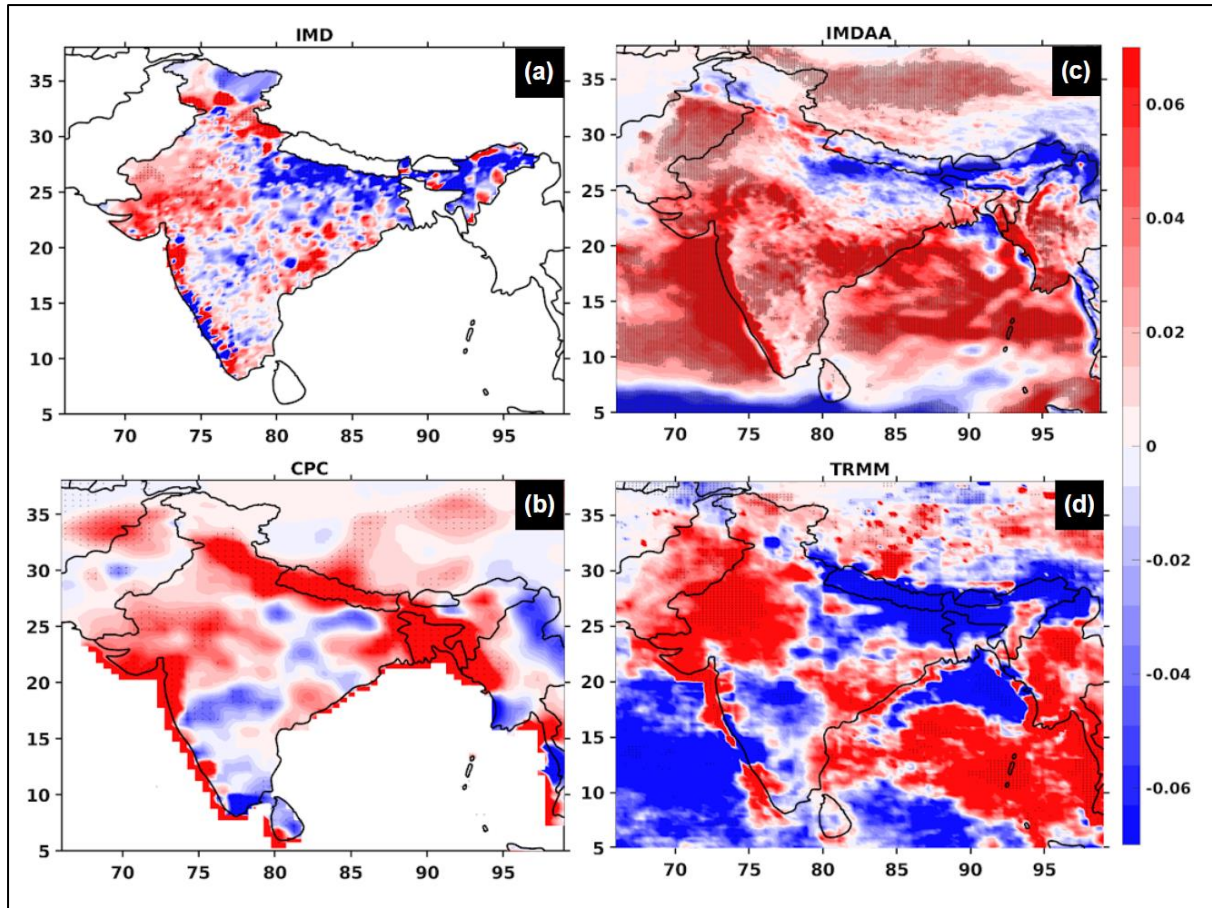


Figure 4: Trend in seasonal (JJAS) precipitation as produced by IMD (a), CPC (b), IMDAA (c) and TRMM (d). Dots represent trends with 95% significance level. Data period for TRMM is 1998-2018 (21 years) while for others it is, 1979-2018 (40 years).

All the datasets except IMD show non-significant increasing trends in the area averaged mean ISM precipitation over MCR (Figure 5a). IMDAA shows the highest significance level of 90%. For Northwest India (Figure 5b), all the datasets show increasing trends, of which CPC has the highest significance of 99%. These findings are in contrast to a study by Kulkarni et al., 2020 reporting a decrease in summer monsoon mean rainfall over the areas of Indo-Gangetic Plains and Roxy et al., 2017 reporting a decreasing trend in mean ISM precipitation over Central India for the period of 1951-2015.

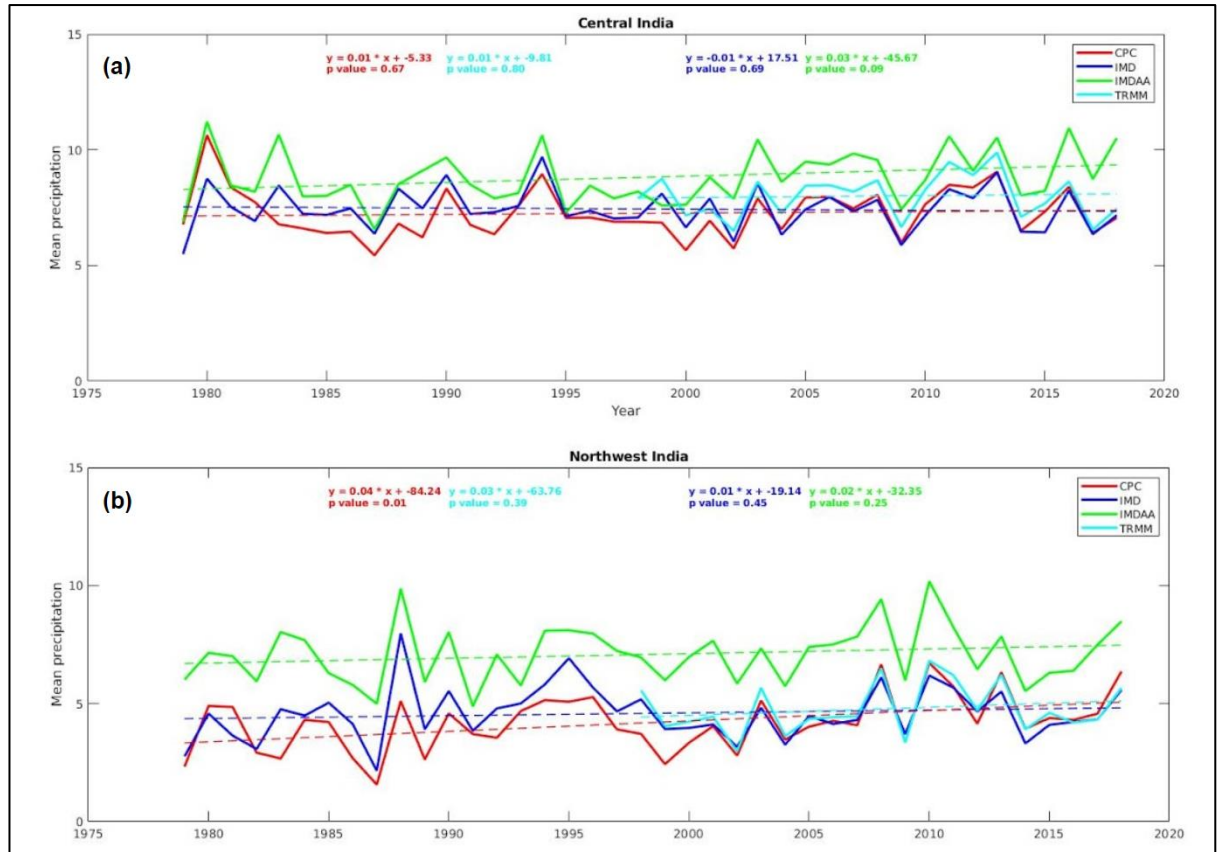


Figure 5: Trends in area-averaged seasonal mean precipitation over MCR (a) and Northwest India (b) as produced by IMDAA, IMD, CPC and TRMM. Data period for TRMM is 1998-2018 (21 years) while for others it is, 1979-2018 (40 years).

Figure 6 shows the trends in monthly mean precipitation (mm/day) for each month of ISM as produced by IMD, IMDAA, CPC and TRMM. All the datasets show significant increasing trends over Northwest India for the month of June and September. July has mostly decreasing trends by all the datasets while for the month of August, except IMD, all show non-significant increasing trends over Northwest India. Decreasing trends in July might be due to the declining of the vertical shear of zonal wind ($0.1 \text{ m s}^{-1} \text{ yr}^{-1}$) and thus causing the weakening of baroclinic instability (J. Shukla, 1978). The weakening of baroclinic instability will lead to decrease in the formation of monsoon convective systems and associated rainfall. For MCR, all the datasets show mixed trends in June followed by significant increasing trends in July. For the month of August, IMD, IMDAA and CPC show a decreasing trend over most of the MCR with TRMM disagreeing. For the month of September, IMD and IMDAA show an increasing trend while CPC and TRMM show a decreasing trend over most of the MCR.

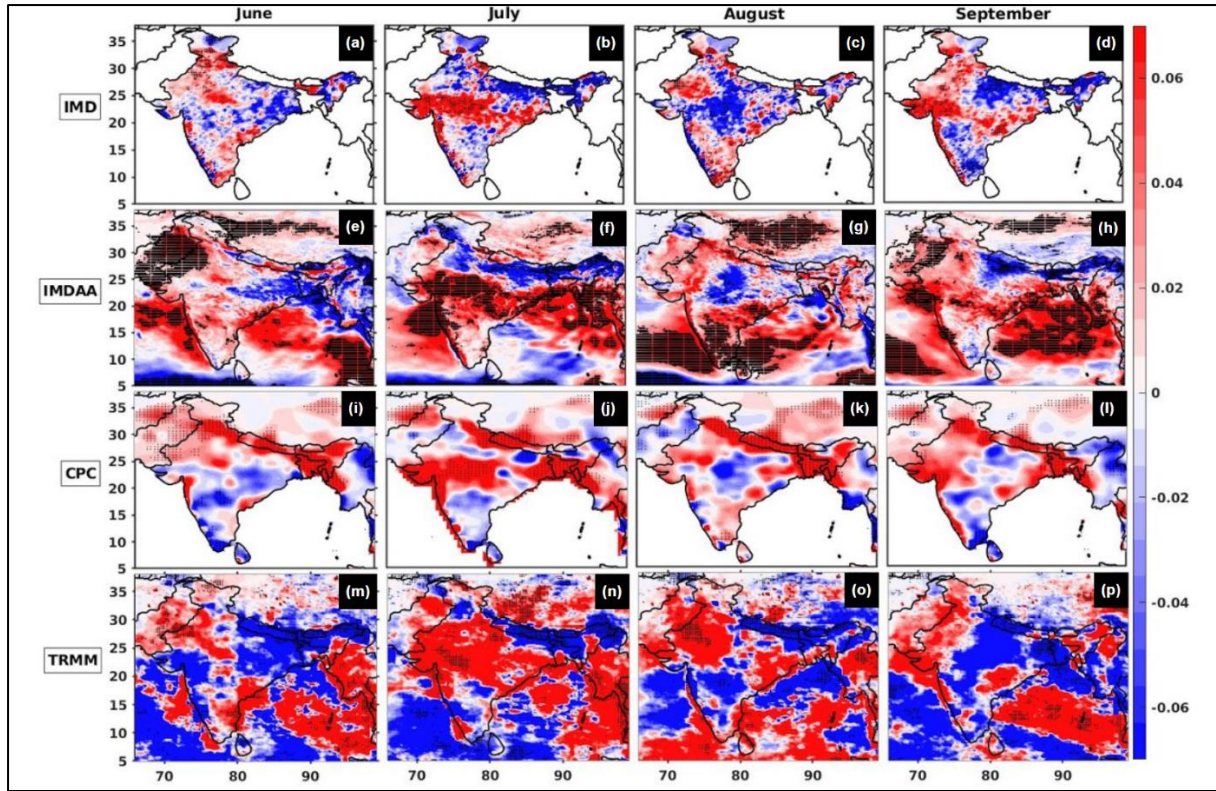


Figure 6: Monthly (June, July, August and September) mean precipitation trends (mm/day/year) as produced by IMD (a-d), IMDAA (e-h), CPC (i-l) and TRMM (m-p). Cross markers (x) indicate trends with 95% significance level. Data period for TRMM is 1998-2018 (21 years) while for others it is, 1979-2018 (40 years).

3.2. Large scale Circulation characteristics of ISM

Indian monsoon has regular characteristics of winds with little inter-seasonal changes (Ramage, 1971 as cited in Ashrit et al., 2020). The ISM is basically associated with important circulation systems such as the heat low (shallow system), the monsoon trough (deep dynamical system), Tibetan anticyclone, upper tropical Easterly Jet (TEJ), and low-level jet (LLJ). Here we analyse some of such typical characteristics such as winds at different pressure levels, mean sea level pressure, vorticity, moisture transport and tropospheric temperature.

Upper level (200 hPa) winds (Figure 7a) show IMDAA well capturing the observed anticyclonic circulation at 25° N with westerlies to the north and easterlies to the south. The wind speeds are also similar to ERA5 (Figure 7d) though IMDAA seems to have weaker easterlies over western equatorial region (Figure 7g). 850

hPa winds (Figure 7b) show that IMDAA realistically represents the cross-equatorial jet stream (LLJ) near the African coast i.e., the Somali jet and the strong westerlies over Arabian Sea, Bay of Bengal and Peninsular India. The strength of the Somali jet in the lower troposphere is a crucial dynamic factor influencing the strength of the ISM rainfall because it transports moisture from the ocean to the Indian subcontinent and the Bay of Bengal (Joseph & Sijikumar, 2004). Comparison with ERA5, however, shows a weaker Somali jet in IMDAA (Figure 7h). IMDAA also well captures the thermal land-sea contrast between Indian subcontinent and Northern Indian ocean during the monsoon as is evident from the MSLP (Figure 7c). Regions of Himalayas, Tibetan plateau and some regions of Middle East, however, show high underestimation of MSLP in IMDAA as compared to ERA5.

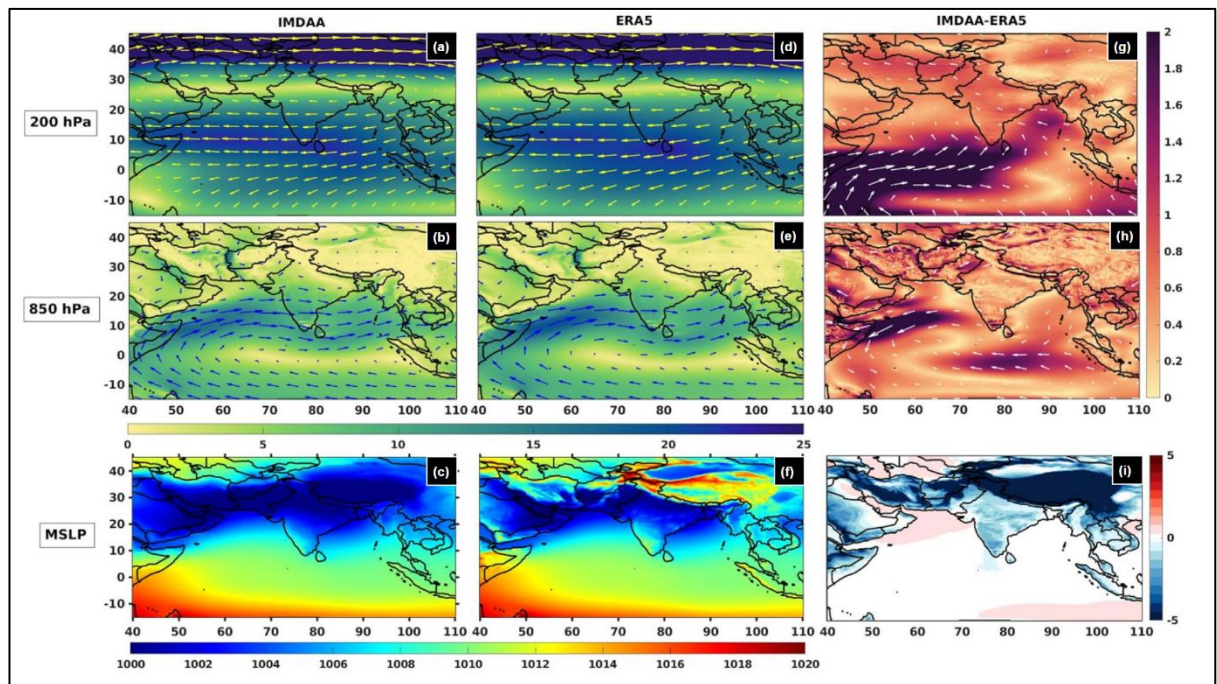


Figure 7: Spatial distribution of mean winds at 200 hPa (m/s), 850 hPa (m/s) and mean sea level pressure (MSLP; hPa) from IMDAA (a, b and c) and ERA5 (d, e and f) for the period 1979-2018. The difference between the two datasets is plotted (g, h and i).

IMDAA produces similar picture of vorticity at 850 hPa during ISM as ERA5 with some differences here and there (Figure 8 a, c and e). Particularly over Northwest India, IMDAA shows more negative vorticity than ERA5. The spatial pattern of moisture transport during ISM, the cross-equatorial transport of moisture from

southern to northern hemisphere through Somali jet, from Arabian sea to Indian mainland & Bay of Bengal and from Bay of Bengal to regions of Southeast Asia are all well captured by IMDAA (Figure 8b). The magnitudes of moisture transport over Indian ocean are however weakly represented in IMDAA as compared to ERA5 (Figure 8f).

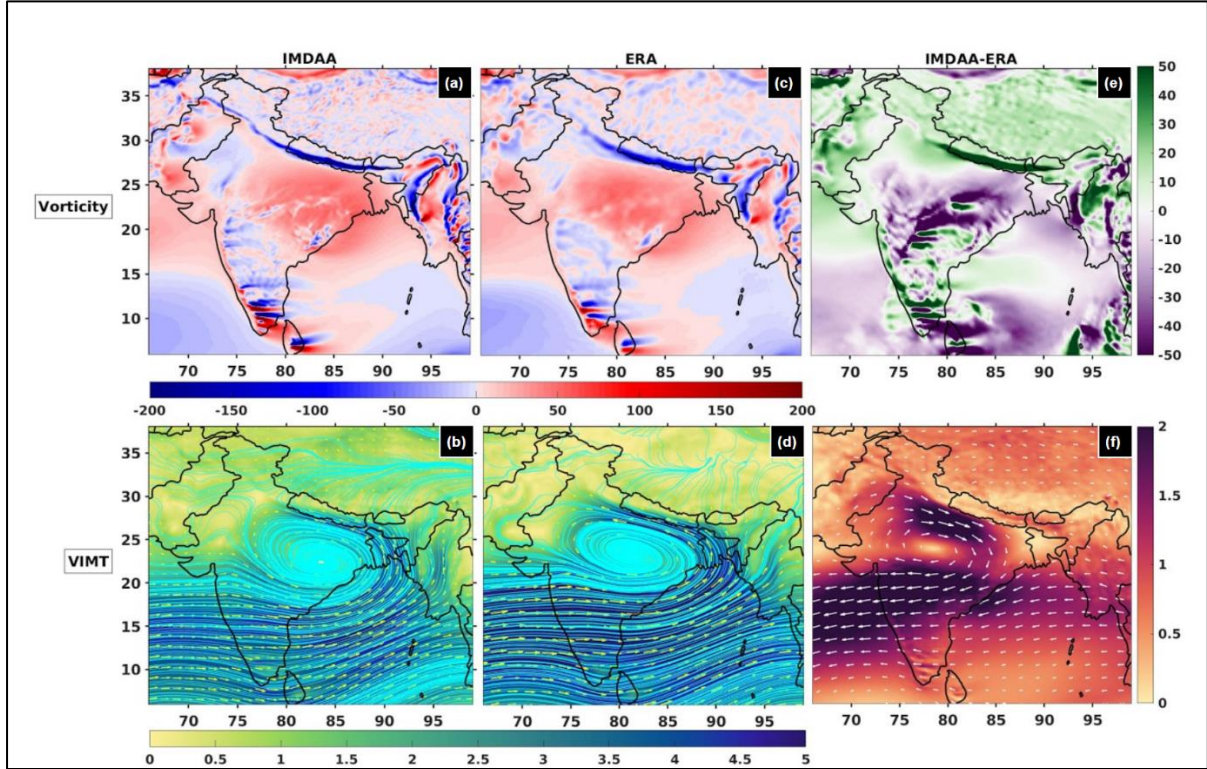


Figure 8: Mean ISM vorticity at 850 hPa (s⁻¹) and vertically integrated (between 1000 and 200 hPa) moisture transport (kg m⁻¹ s⁻¹) as captured by IMDAA (a and b), ERA5 (c and d) and the difference between two datasets (e and f).

IMDAA seems to underestimate the tropospheric temperature during ISM over its entire spatial domain in comparison to ERA5 (Figure 9). There is relatively more agreement between IMDAA and ERA5 over Tibetan plateau than the rest of the spatial domain. The tropospheric temperature has significant influence on climate variability around the globe and is an important and widely used indicator of climate change. Studies have shown that the tropospheric temperature over Asia has lowered in recent decades while it has increased over the tropical Indian ocean resulting in reduced meridional and zonal land-sea thermal contrasts, and weakening of Asian summer monsoon (Kulkarni et al., 2020; Vaid & San Liang, 2015).

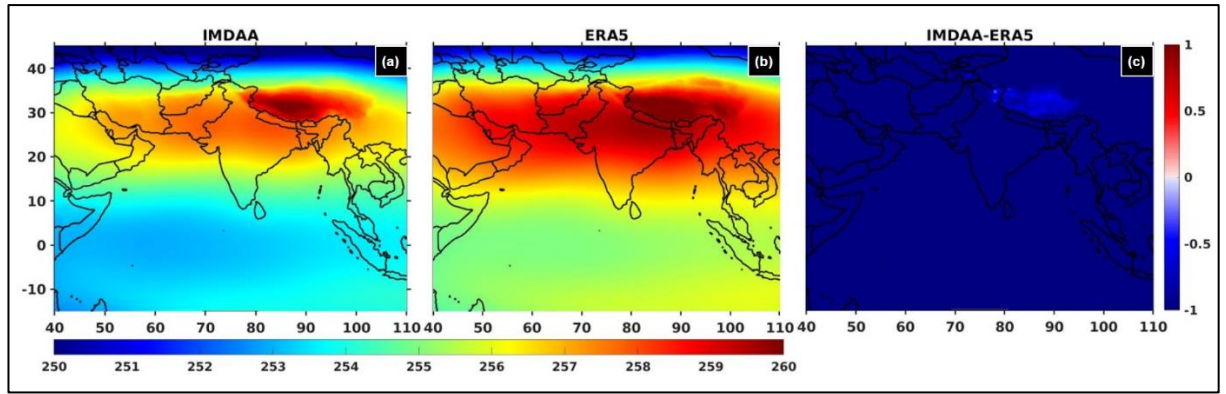


Figure 9: Mean ISM tropospheric temperature (between 700 and 200 hPa) as captured by IMDAA (a), ERA5 (b) and the difference between the two (c).

(Figure 10) Seasonal mean meridional distribution of easterly wind shear (200 hPa - 850 hPa) which is one of the key parameters for the northward propagation of the convection (Attada et al., 2018). IMDAA exhibits good agreement with ERA5 reanalysed fields. However, tropospheric temperature (averaged between 700 and 200 hPa) seems to be underestimated in IMDAA while overestimating vertically integrated specific humidity (1000 to 850 hPa) during ISM. Vertical profile of diabatic heating is plotted over the MCR and Northwest India from ERA5 but not for IMDAA as it does not have the required variable of vertical velocity at this point of time. Diabatic heating represents the heat sources associated with phase changes (e.g. Mukhopadhyay et al., 2010). Thus, it represents the heat exchange between air parcel and its surroundings, in contrast to the adiabatic heating/cooling in which air parcel heats/cools solely because of the pressure variations. Diabatic heating associated with tropical precipitation is an important factor driving the circulation and its vertical profile depends upon the relative presence of the two regions of MCSs: convective and stratiform. In convective regions of MCSs, the heating profile has positive heating throughout the troposphere with a maximum in the mid troposphere, while, in stratiform regions, there is an upper-level heating and cooling below the melting level (Hagos et al., 2010; Hong et al., 1999; Lang et al., 2003; Schumacher & Houze, 2003). Over the MCR (Figure 10d), diabatic heating is peak in the middle troposphere where the maximum latent heat releases. This heating further enhances the tropospheric temperature gradient then sustains the ISM circulation. In the case of Northwest India, the diabatic heating profile is weaker compared to MCR as the rainfall is 30% lesser than the MCR. However, it is

important to mention that the maximum peak is also noticeable in the mid-troposphere.

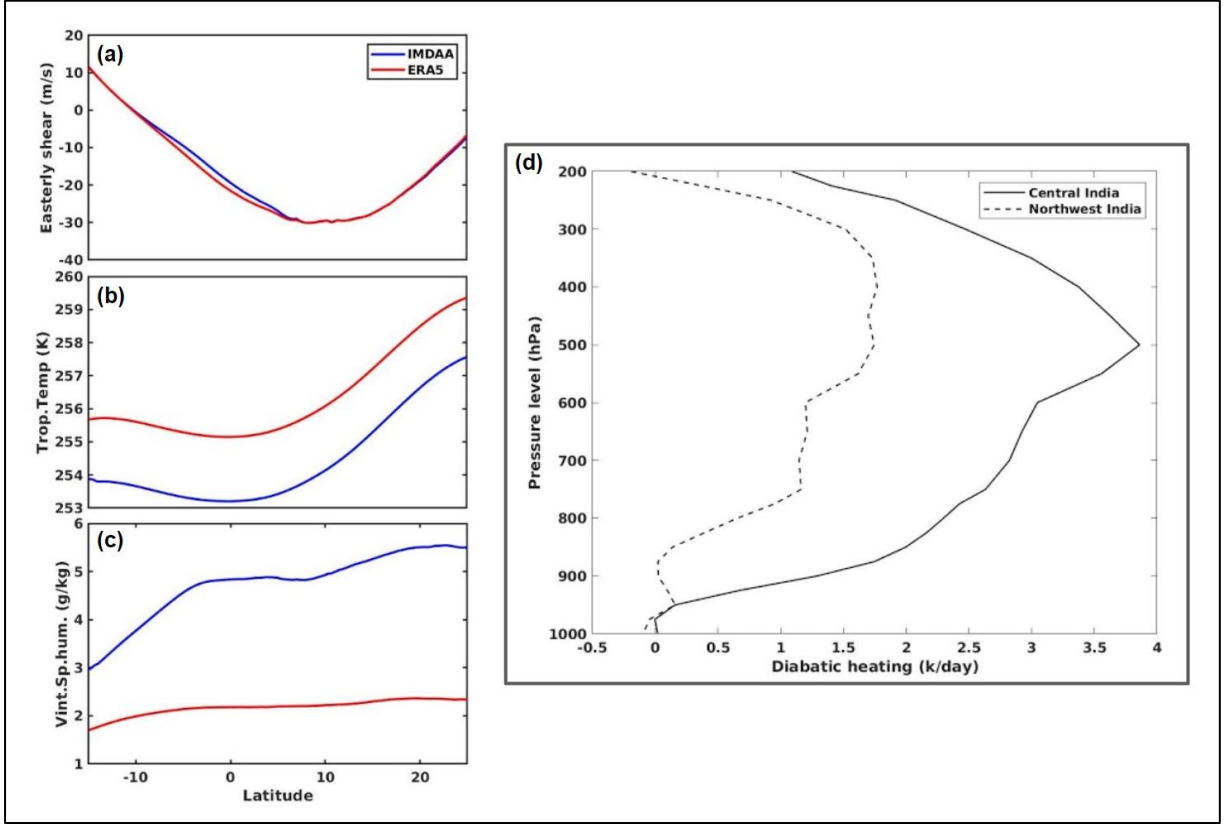


Figure 10: Mean meridional distribution of easterly wind shear (a), tropospheric temperature (b) and vertically integrated specific humidity (c) averaged between 60°E and 100°E during ISM as captured by IMDAA (solid blue) and ERA5 (solid red). (d) Vertical profile of diabatic heating over MCR (solid black) and Northwest India (dashed black) during ISM as captured by ERA5.

3.3. Extreme rainfall events (EREs) during ISM

Given the large impacts of EREs on cultural, social, and economic life of society, it is vital to study characteristics of such events including an assessment of their future evolution (Goswami et al., 2006; Kulkarni et al., 2020; Malik et al., 2016; Roxy et al., 2017). Many climate model studies have suggested a rise in EREs in future in continuation to past increasing trend since 1950 as observed by many observational studies, mostly due to tropospheric warming leading to an enhancement of moisture content of the atmosphere (Goswami et al., 2006;

Kulkarni et al., 2020; Roxy et al., 2017). The aspect of spatial variability of EREs across India remains contested among various studies (Malik et al., 2016; Roxy et al., 2017). Though studies agree upon increasing EREs in MCR, analysis with high resolution reanalysis like IMDAA has not been attempted before and as for Northwest India, contrasting results are reported (Goswami et al., 2006; Malik et al., 2016; Roxy et al., 2017). Thus, we perform the analysis of EREs over MCR and Northwest India using high resolution regional atmospheric reanalysis, IMDAA and compare it with observational trends.

World Meteorological Organization (WMO) recommends to use fixed absolute values since they represent the disaster-causing potential better than percentile values but a fixed threshold for defining EREs is not preferable for a region with high spatial variability in mean climate (Goswami et al., 2006; Roxy et al., 2017). Fixed thresholds can be used for our study regions of MCR and Northwest India because they fall under the homogenous rainfall regions as classified by IMD (Zheng et al., 2016). EREs over MCR are defined as those instances when one day accumulated rainfall over a grid point exceeds 150 mm while for Northwest India, the threshold is fixed at 109 mm. To produce the atmospheric characteristics prevalent during widespread events, IMDAA and ERA5 make use of widespread events from IMDAA and IMD, respectively. Plots of circulation variables from ERA5 make use of widespread events from IMD and will be referred to as ERA_IMD.

3.3.1. Monsoon Core Region (MCR)

A. Spatio-temporal trends

Both IMD and IMDAA show mixed trends in EREs (>150 mm/day) over the study region of MCR for the last 40 years since 1979 (Figure 11). However, they both agree upon the presence of significant declining trends in EREs near Himalayan foothills in Uttar Pradesh and increasing trends along the coast of West Bengal and Orissa. Both the datasets show absence of any trends positive or negative in areas of Jammu and Kashmir, Ladakh, Rajasthan and Peninsular India. Widespread events in the MCR study region show non-significant increasing trend according to

IMD (2.4 events in last 40 years) and no trend according to IMDAA. Both the datasets represent an oscillatory behaviour in no. of widespread events occurring in an year though, IMDAA records more widespread events in a given year as compared to IMD.

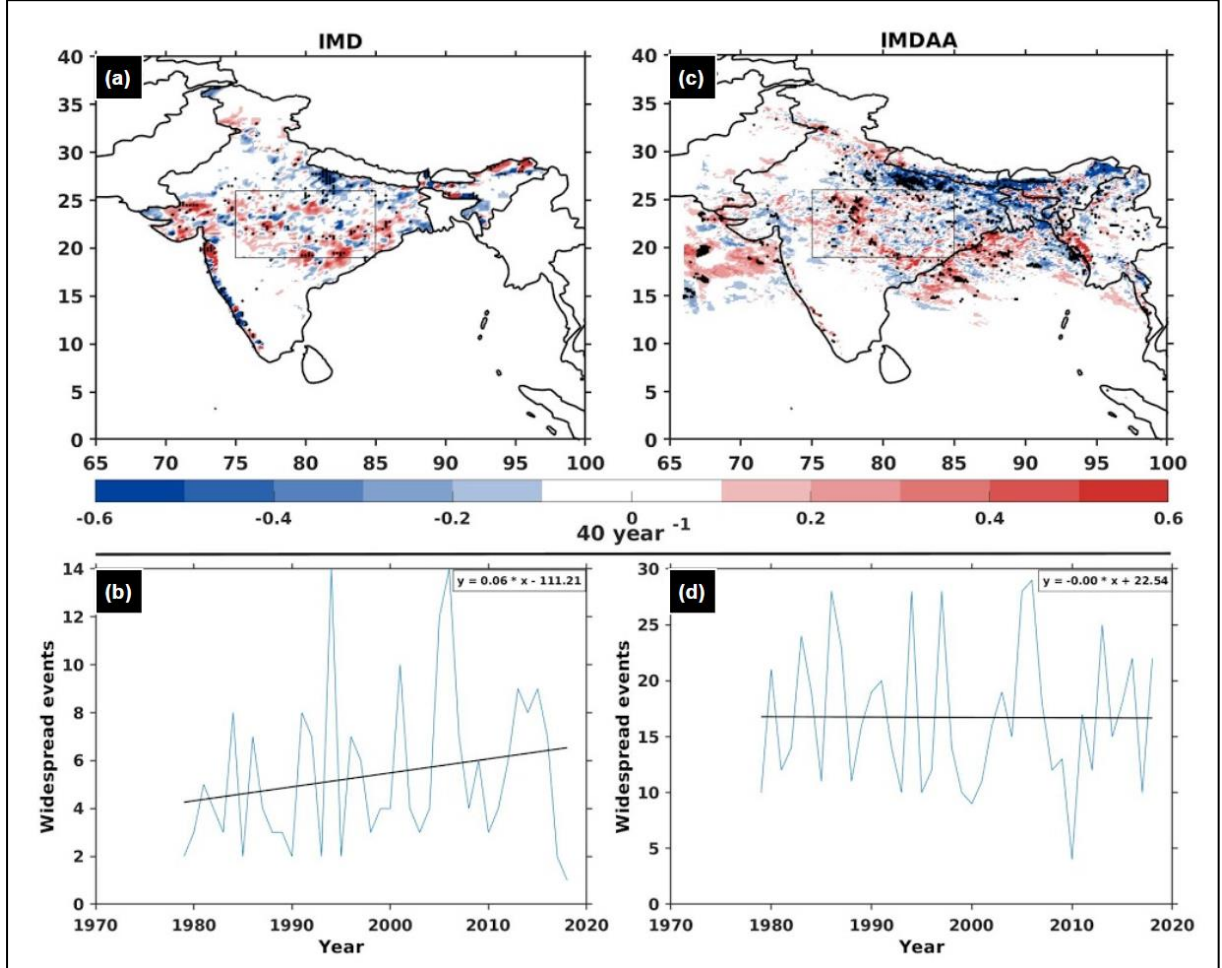


Figure 11: Linear trends in frequency of EREs (more than 150 mm/day) and widespread events over MCR as produced by IMD (a and b) and IMDAA (c and d). The box in a and c represent the MCR region taken to calculate the widespread events in b and d. Trend values are in $\text{mm day}^{-1} 40 \text{ year}^{-1}$.

B. Circulation characteristics of EREs

Further, we explore the circulation characteristics associated with these EREs over the MCR using IMDAA and ERA5 data. Figure 12 shows winds at 200 and 850 hPa during widespread events over MCR. IMDAA well captures the cyclonic circulation at 850 hPa over MCR though it is weaker as compared to ERA_IMD. The strong westerlies at 850 hPa over Arabian sea, Peninsular India and Bay of

Bengal are also captured well by IMDAA though with some underestimation over Arabian Sea. Winds at 200 hPa during widespread events are almost same as those during any time during ISM though anticyclonic circulation has shifted northwards compared to mean conditions. IMDAA also exhibits strong westerlies at 200 hPa over Tibetan plateau as compared to ERA_IMD, which might be due to strong topographic forcing.

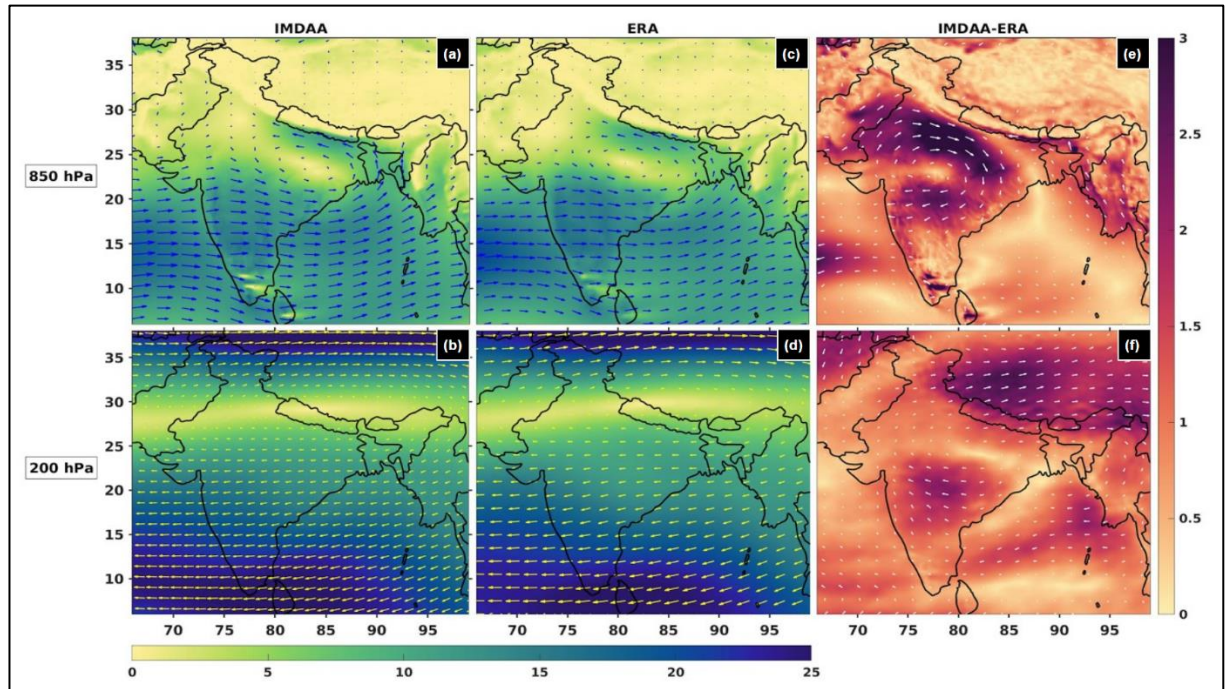


Figure 12: Winds at 850 hPa (m/s) and 200 hPa (m/s) during widespread events over MCR from IMDAA (a and b) and IMD (c and d). The difference between the two is also plotted (e and f).

(Figure 13) Both IMDAA and ERA_IMD show strong positive low level vorticity (cyclonic circulation) prevalent over MCR during widespread events with IMDAA mostly underestimating it over the study region. Vertically integrated moisture transport (streamlines and dark shadings) during widespread events over MCR depicts that such events are fed by both Arabian Sea and Bay of Bengal. IMDAA, however, underestimates contribution from both Arabian Sea and Bay of Bengal as compared to observations.

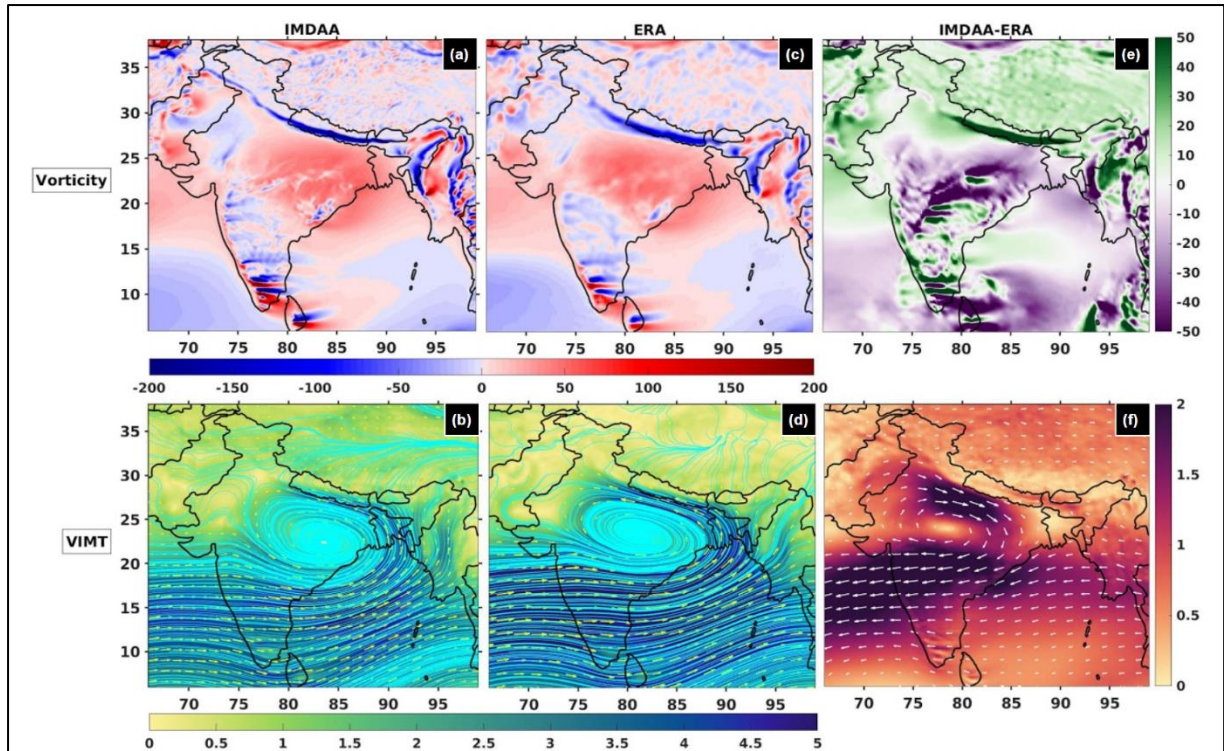


Figure 13: Vorticity at 850 hPa (s^{-1}) and VIMT for 1000 to 200 hPa ($kg\ m^{-1}\ s^{-1}$) during widespread events over MCR from IMDAA (a and b) and IMD (c and d). The difference between the two is also plotted (e and f).

3.3.2. Northwest India

A. Spatio-temporal trends in EREs

Northwest India is a centre to intensive urbanization and agriculture, which is mostly dependent on ground water given the semi-arid nature of climate of the area. A proper assessment of EREs is thus required for considering optimum adaption strategies for both sustainable use of water resources and adverse impacts of such events which include flash floods, crop damages etc (Goswami et al., 2006; Pingale et al., 2014). Both IMD and IMDAA show mixed trends in EREs over the study region of Northwest India for the last 40 years since 1979 (Figure 14). Both, however, again agree upon the presence of significant declining trends in EREs near Himalayan foothills in Uttar Pradesh and Bihar. Widespread events in Northwest India from IMD show no trend with a non-significant increasing trend from IMDAA.

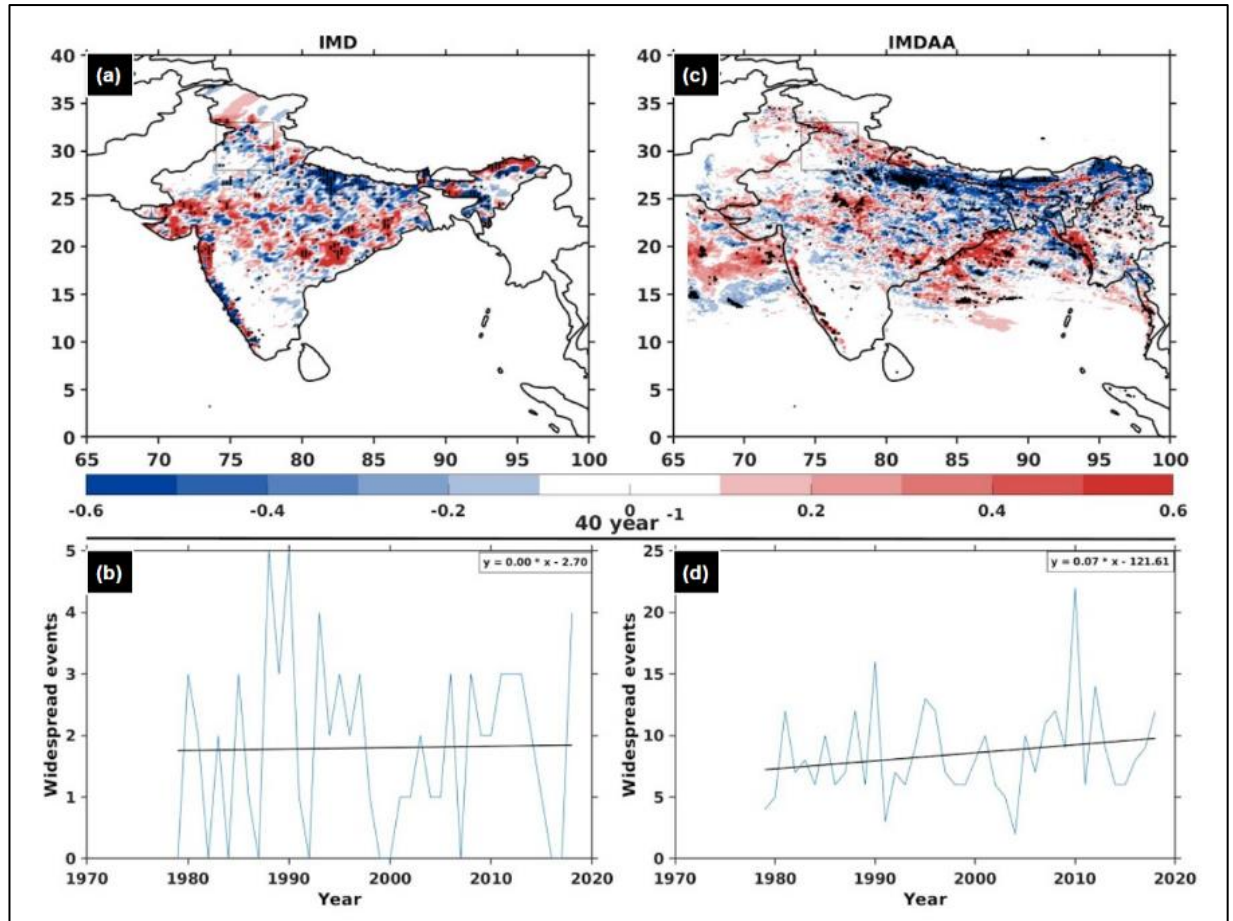


Figure 14: Linear trends in frequency of EREs (more than 109 mm/day) and widespread events over Northeast India from IMD (a and b) and IMDAA (c and d). The box in a and c represent the Northwest India region taken to calculate the widespread events in b and d. Trend values are in mm day⁻¹ 40 year⁻¹.

B. Circulation characteristics of EREs

We further analyse the circulation characteristics of these EREs over Northwest India using IMDAA and ERA5. 850 hPa winds during widespread events by IMDAA show some local cyclonic circulation over regions of Northwest India and Pakistan along with strong westerlies over Arabian Sea, Peninsular India and Bay of Bengal (Figure 15). ERA_IMD, however, seems to be rejecting the idea of local cyclonic circulation. 200 hPa winds show slight northward shift in the anticyclonic circulation compared to mean conditions with IMDAA showing weaker westerlies over Northwest India and stronger easterlies over Bay of Bengal, Peninsular India and Arabian Sea. Both IMDAA and ERA_IMD show positive vorticity (Figure 16

a, c and e) over most of the Northwest India, MCR, Arabian Sea and Bay of Bengal with IMDAA being on the lower side. Vertically integrated moisture transport streamlines (Figure 16 b, d and f) show both Arabian Sea and Bay of Bengal being the sources of moisture for widespread events over Northwest India. IMDAA, however, underestimates the contribution from Arabian Sea.

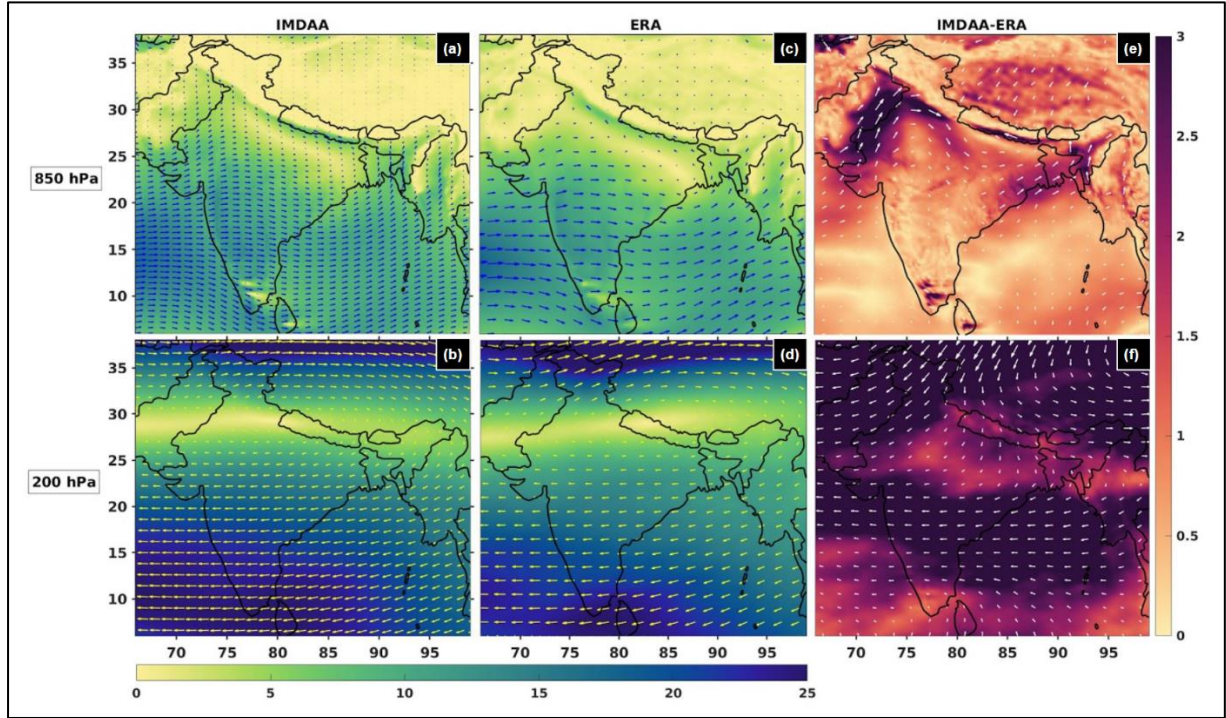


Figure 15: Winds at 850 hPa (m/s) and 200 hPa (m/s) during widespread events over Northwest India from IMDAA (a and b) and IMD (c and d). The difference between the two is also plotted (e and f).

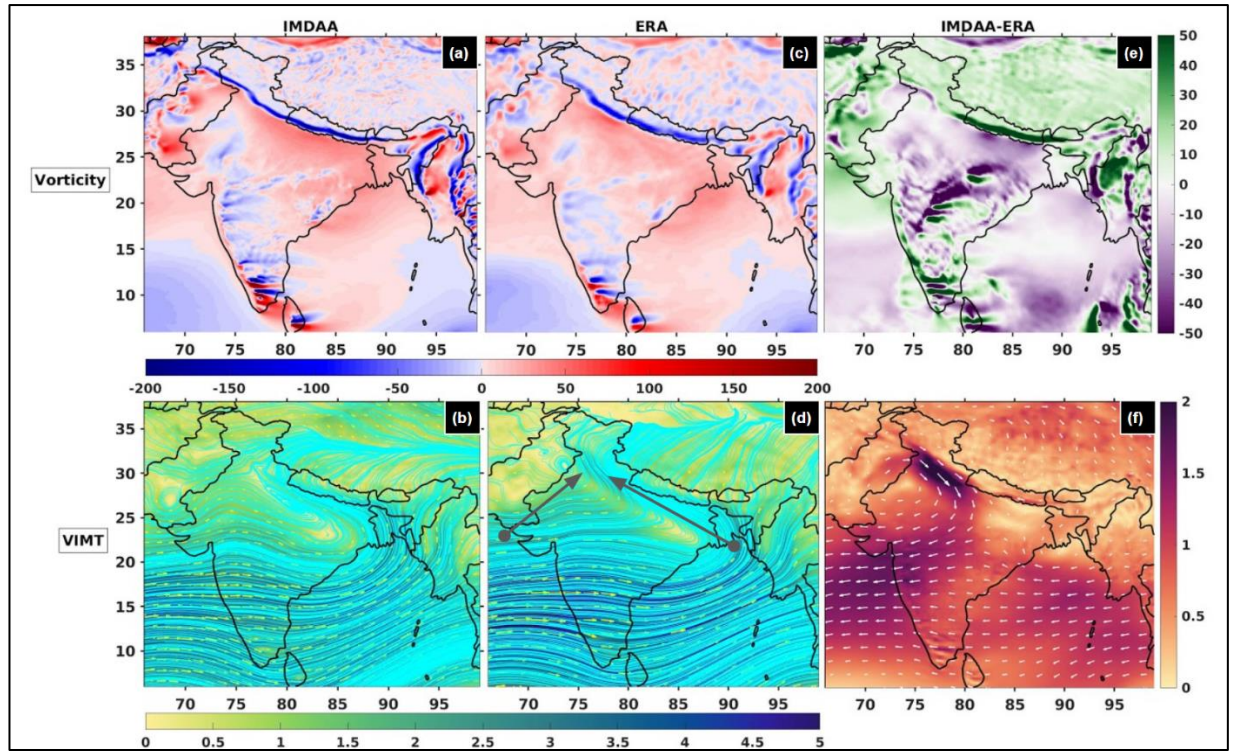


Figure 16: Vorticity at 850 hPa (s^{-1}) and VIMT for 1000 to 200 hPa ($kg\ m^{-1}\ s^{-1}$) during widespread events over Northwest India from IMDAA (a and b) and IMD (c and d). The difference between the two is also plotted (e and f).

Chapter 4

Conclusion

This study examines the performance of IMDAA, the first high-resolution (12 km) atmospheric reanalysis over the Indian subcontinent, with respect to precipitation and associated atmospheric circulation characteristics during ISM using IMD, ERA5, CPC and TRMM datasets for the period of 1979 to 2018. Further, we have analysed the linear trends in mean precipitation, including sub-seasonal (monthly) scales as well as extreme rainfall events happening during monsoon across the country focusing on two study regions of Northwest India (semi-arid climate type) and MCR (wet climate type). Following are the major findings of the study:

1. IMDAA successfully captures the spatio-temporal variation in precipitation across India during ISM with some overestimation perhaps due to its higher resolution than other datasets used for comparison.
2. With respect to precipitation, IMDAA shows highest correlation and agreement with IMD compared to CPC and TRMM, and that is also higher over MCR (0.96) than Northwest India (0.81).
3. IMDAA realistically represents the monsoon circulation features such as Low Level Jet, Cross-Equatorial Flow, Monsoon Trough, Tropical Easterly Jet, Tibetan Anticyclone. Finer details of moisture transport is accurately obtained by IMDAA, which would be useful to track the regional moisture sources.
4. Mean sea level pressure is better captured over India by IMDAA but with significant discrepancies over Tibetan plateau and Middle east. Tropospheric temperature is underestimated at least by 1° C everywhere over the spatial domain of IMDAA

5. Spatial trend in seasonal mean precipitation show increasing trend over Northwest India but no homogeneous trend is noticed over MCR.
6. Monthly mean precipitation over Northwest India shows increasing trends for the months of June and September along with declining trend for July. Over MCR, monthly mean precipitation shows homogeneous significant increasing trends for July with non-homogeneous trends for other monsoon months, which might be due to more number of monsoon depressions formation over the Bay of Bengal.
7. No homogeneous and significant trends in EREs and widespread events for the last 40 years are found over either of the study regions by either IMDAA or IMD.

Bibliography

- Arjun, K. M. (2013). Indian Agriculture-Status, Importance and Role in Indian Economy. In *International Journal of Agriculture and Food Science Technology* (Vol. 4, Issue 4).
- Ashrit, R., Indira Rani, S., Kumar, S., Karunasagar, S., Arulalan, T., Francis, T., Routray, A., Laskar, S. I., Mahmood, S., Jerney, P., Maycock, A., Renshaw, R., George, J. P., & Rajagopal, E. N. (2020). IMDAA Regional Reanalysis: Performance Evaluation During Indian Summer Monsoon Season. *Journal of Geophysical Research: Atmospheres*, 125(2).
<https://doi.org/10.1029/2019JD030973>
- Attada, R., Parekh, A., Chowdary, J. S., & Gnanaseelan, C. (2018). Reanalysis of the Indian summer monsoon: four dimensional data assimilation of AIRS retrievals in a regional data assimilation and modeling framework. *Climate Dynamics*, 50(7–8). <https://doi.org/10.1007/s00382-017-3781-z>
- Gadgil, S. (2018). The monsoon system: Land–sea breeze or the ITCZ? *Journal of Earth System Science*, 127(1). <https://doi.org/10.1007/s12040-017-0916-x>
- Goswami, B. N., Venugopal, V., Sangupta, D., Madhusoodanan, M. S., & Xavier, P. K. (2006). Increasing trend of extreme rain events over India in a warming environment. *Science*, 314(5804). <https://doi.org/10.1126/science.1132027>
- Hagos, S., Zhang, C., Tao, W. K., Lang, S., Takayabu, Y. N., Shige, S., Katsumata, M., Olson, B., & L'ecuyer, T. (2010). Estimates of tropical diabatic heating profiles: Commonalities and uncertainties. *Journal of Climate*, 23(3). <https://doi.org/10.1175/2009JCLI3025.1>
- Halpert, M. S., & Bell, G. D. (1997). Climate Assessment for 1996. *Bulletin of the American Meteorological Society*, 78(5). [https://doi.org/10.1175/1520-0477\(1997\)078<1038:caf>2.0.co;2](https://doi.org/10.1175/1520-0477(1997)078<1038:caf>2.0.co;2)
- Hersbach, H., Bell, B., Berrisford, P., Hirahara, S., Horányi, A., Muñoz-Sabater, J., Nicolas, J., Peubey, C., Radu, R., Schepers, D., Simmons, A., Soci, C., Abdalla, S., Abellan, X., Balsamo, G., Bechtold, P., Biavati, G., Bidlot, J.,

- Bonavita, M., ... Thépaut, J. N. (2020). The ERA5 global reanalysis. *Quarterly Journal of the Royal Meteorological Society*, 146(730).
<https://doi.org/10.1002/qj.3803>
- Hong, Y., Kummerow, C. D., & Olson, W. S. (1999). Separation of convective and stratiform precipitation using microwave brightness temperature. *Journal of Applied Meteorology*, 38(8). [https://doi.org/10.1175/1520-0450\(1999\)038<1195:SOCASP>2.0.CO;2](https://doi.org/10.1175/1520-0450(1999)038<1195:SOCASP>2.0.CO;2)
- Joseph, P. V., & Sijikumar, S. (2004). Intraseasonal variability of the low-level jet stream of the Asian summer monsoon. *Journal of Climate*, 17(7).
[https://doi.org/10.1175/1520-0442\(2004\)017<1449:IVOTLJ>2.0.CO;2](https://doi.org/10.1175/1520-0442(2004)017<1449:IVOTLJ>2.0.CO;2)
- Kim, J., Sanjay, J., Mattmann, C., Boustani, M., Ramarao, M. V. S., Krishnan, R., & Waliser, D. (2015). Uncertainties in estimating spatial and interannual variations in precipitation climatology in the India-Tibet region from multiple gridded precipitation datasets. *International Journal of Climatology*, 35(15).
<https://doi.org/10.1002/joc.4306>
- Kulkarni, A., Sabin, T. P., Chowdary, J. S., KoteswaraRao, K., Priya, P., Gandhi, N., Bhaskar, P., Buri, V. K., & Sabade, S. S. (2020). Precipitation changes in India. In *Assessment of Climate Change over the Indian Region: A Report of the Ministry of Earth Sciences (MoES), Government of India*.
https://doi.org/10.1007/978-981-15-4327-2_3
- Lang, S., Tao, W. K., Simpson, J., & Ferrier, B. (2003). Modeling of convective-stratiform precipitation processes: Sensitivity to partitioning methods. *Journal of Applied Meteorology*, 42(4). [https://doi.org/10.1175/1520-0450\(2003\)042<0505:MOCSP>2.0.CO;2](https://doi.org/10.1175/1520-0450(2003)042<0505:MOCSP>2.0.CO;2)
- Malik, N., Bookhagen, B., & Mucha, P. J. (2016). Spatiotemporal patterns and trends of Indian monsoonal rainfall extremes. *Geophysical Research Letters*, 43(4). <https://doi.org/10.1002/2016GL067841>
- Mcbride, J. L., & Ebert, E. E. (2000). Verification of quantitative precipitation forecasts from operational numerical weather prediction models over Australia. *Weather and Forecasting*, 15(1). [https://doi.org/10.1175/1520-0434\(2000\)015<0103:VOQPFF>2.0.CO;2](https://doi.org/10.1175/1520-0434(2000)015<0103:VOQPFF>2.0.CO;2)

- Misra, V., Bhardwaj, A., & Mishra, A. (2018). Local onset and demise of the Indian summer monsoon. *Climate Dynamics*, 51(5–6).
<https://doi.org/10.1007/s00382-017-3924-2>
- Mukhopadhyay, P., Taraphdar, S., Goswami, B. N., & Krishnakumar, K. (2010). Indian summer monsoon precipitation climatology in a high-resolution regional climate model: Impacts of convective parameterization on systematic biases. *Weather and Forecasting*, 25(2).
<https://doi.org/10.1175/2009WAF2222320.1>
- P Sabin, T., Krishnan, R., Ghattas, J., Denvil, S., Dufresne, J. L., Hourdin, F., & Pascal, T. (2013). High resolution simulation of the South Asian monsoon using a variable resolution global climate model. *Climate Dynamics*, 41(1).
<https://doi.org/10.1007/s00382-012-1658-8>
- Perez, J. M., Aponte-Bermudez, L. D., Morell, J. M., & Rodriguez, E. (2016). CariCOOS: Real-time data validation of high-resolution wind forecast. *OCEANS 2015 - MTS/IEEE Washington*.
<https://doi.org/10.23919/oceans.2015.7404368>
- Pingale, S. M., Khare, D., Jat, M. K., & Adamowski, J. (2014). Spatial and temporal trends of mean and extreme rainfall and temperature for the 33 urban centers of the arid and semi-arid state of Rajasthan, India. *Atmospheric Research*, 138. <https://doi.org/10.1016/j.atmosres.2013.10.024>
- Raju, A., Parekh, A., Chowdary, J. S., & Gnanaseelan, C. (2015). Assessment of the Indian summer monsoon in the WRF regional climate model. *Climate Dynamics*, 44(11–12). <https://doi.org/10.1007/s00382-014-2295-1>
- Rani, S. I., Arulalan, T., George, J. P., & Rajagopal, E. N. (n.d.). *IMDAA : High Resolution Satellite-era Reanalysis for the Indian Monsoon Region*.
<https://doi.org/10.1175/JCLI-D-20-0412.1>
- Rao, D. N., Ratnam, M. V., Mehta, S., Nath, D., Basha, S. G., Rao, V. V. M. J., Murthy, B. V. K., Tsuda, T., & Nakamura, K. (2009). Validation of the COSMIC radio occultation data over gadanki (13.48°N. 79.2°E): A tropical region. *Terrestrial, Atmospheric and Oceanic Sciences*, 20(1).
[https://doi.org/10.3319/TAO.2008.01.23.01\(F3C\)](https://doi.org/10.3319/TAO.2008.01.23.01(F3C))

- Roxy, M. K., Ghosh, S., Pathak, A., Athulya, R., Mujumdar, M., Murtugudde, R., Terray, P., & Rajeevan, M. (2017). A threefold rise in widespread extreme rain events over central India. *Nature Communications*, 8(1).
<https://doi.org/10.1038/s41467-017-00744-9>
- Roy, S. Sen, & Balling, R. C. (2004). Trends in extreme daily precipitation indices in India. *International Journal of Climatology*, 24(4).
<https://doi.org/10.1002/joc.995>
- Schumacher, C., & Houze, R. A. (2003). Stratiform rain in the tropics as seen by the TRMM precipitation radar. *Journal of Climate*, 16(11).
[https://doi.org/10.1175/1520-0442\(2003\)016<1739:SRITTA>2.0.CO;2](https://doi.org/10.1175/1520-0442(2003)016<1739:SRITTA>2.0.CO;2)
- Shukla, J. (1978). CISK-Barotropic-Baroclinic Instability and the Growth of Monsoon Depressions. *Journal of the Atmospheric Sciences*, 35(3).
[https://doi.org/10.1175/1520-0469\(1978\)035<0495:cbbiat>2.0.co;2](https://doi.org/10.1175/1520-0469(1978)035<0495:cbbiat>2.0.co;2)
- Shukla, R. P., & Huang, B. (2016). Interannual variability of the Indian summer monsoon associated with the air–sea feedback in the northern Indian Ocean. *Climate Dynamics*, 46(5–6). <https://doi.org/10.1007/s00382-015-2687-x>
- Soman, M. K., & Kumar, K. K. (1993). Space-time evolution of meteorological features associated with the onset of Indian summer monsoon. *Monthly Weather Review*, 121(4). [https://doi.org/10.1175/1520-0493\(1993\)121<1177:STEOMF>2.0.CO;2](https://doi.org/10.1175/1520-0493(1993)121<1177:STEOMF>2.0.CO;2)
- Thornes, J. E., & Stephenson, D. B. (2001). How to judge the quality and value of weather forecast products. *Meteorological Applications*, 8(3).
<https://doi.org/10.1017/S1350482701003061>
- Vaid, B. H., & San Liang, X. (2015). Tropospheric temperature gradient and its relation to the South and East Asian precipitation variability. *Meteorology and Atmospheric Physics*, 127(5). <https://doi.org/10.1007/s00703-015-0385-1>
- Zandler, H., Haag, I., & Samimi, C. (2019). Evaluation needs and temporal performance differences of gridded precipitation products in peripheral mountain regions. *Scientific Reports*, 9(1). <https://doi.org/10.1038/s41598-019-51666-z>
- Zhang, Q., Pan, Y., Wang, S., Xu, J., & Tang, J. (2017). High-Resolution

Regional Reanalysis in China: Evaluation of 1 Year Period Experiments.

Journal of Geophysical Research: Atmospheres, 122(20).

<https://doi.org/10.1002/2017JD027476>

Zheng, Y., Bourassa, M. A., Ali, M. M., & Krishnamurti, T. N. (2016). Distinctive features of rainfall over the Indian homogeneous rainfall regions between strong and weak Indian summer monsoons. *Journal of Geophysical Research*, 121(10). <https://doi.org/10.1002/2016JD025135>